Many-body theory for charge transfer in atom-surface collisions

Hongxiao Shao and David C. Langreth
Department of Physics and Astronomy, Rutgers University, Piscataway, New Jersey 08855-0849

Peter Nordlander
Department of Physics and Rice Quantum Institute, Rice University, Houston, Texas 77251-1892
(Received 23 June 1993; revised manuscript received 10 January 1994)

A theory for the effect of a strong intra-atomic Coulomb repulsion U on the nonadiabatic transfer of charge between a metallic surface and a moving atomic species is presented. Using slave bosons and a nonequilibrium Green's-function technique, we solve the equations appropriate for the $U = \infty$ problem in the case when either the atom-surface hopping matrix element is small, or the number of degenerate atomic states is large. We generalize the earlier treatment of Langreth and Nordlander (LN) to include off-diagonal self-energies and present a general numerical scheme for the exact solution of the Dyson equations. We verify that our scheme gives the correct answer in several limiting cases where an exact solution is known, and give quantitative predictions of when deviations from these limits become important. These limits include (1) the simple master equation limit for low velocities and weak coupling, (2) the generalized master equation of LN for larger velocities and atom-surface coupling, (3) the approach to thermal equilibrium when the time dependence is removed, and (4) the maintenance of local thermal equilibrium when the energy parameters vary sufficiently slowly. From a calculation of the instantaneous (nonequilibrium) spectral function of the level on the scattering atom, we are able to study the rate of formation of the Kondo and mixed valent resonances near the Fermi level. We find a slow formation rate for such resonances relative to that of the broader parts of the spectral density centered near the bare atom level positions.

I. INTRODUCTION

Charge-transfer phenomena have been observed in many low energy ion-scattering experiments.[1–7] Several experiments[1–4,8] have shown that intra-atomic Coulomb correlation has significant effects on charge transfer. Theoretically, the dynamical interaction between atoms and surfaces is normally described using the time-dependent Anderson model.[9] However, most of the theoretical work on charge transfer processes has neglected the effect of intra-atomic Coulomb correlation.[10–12] Some attempts[12–17] to account for it have been made, but a general and consistent treatment for the problems where multiple tunneling channels can coexist has been lacking.

Recent theoretical calculations have shown that several different atomic states can participate in the charge exchange process between the atom and the surface.[18,19] The final charge state of the atoms can therefore be strongly affected by intra-atomic Coulomb correlation. The conventional spinless theory is inadequate in this situation.

Langreth and Nordlander[20] (LN) extended the slave boson technique of Coleman[21] to the nonequilibrium situation and used it to investigate the effect of large intra-atomic Coulomb correlation on charge transfer dynamics. The nonequilibrium version was based on a Green's function method developed by Kadanoff and Baym[22] and Keldysh.[23] A set of coupled time dependent Dyson equations for the Green's functions associated with the atomic levels and the slave-boson state were derived. An approximate solution was obtained using what was called the semiclassical approximation (SCA).[20] In the SCA, the set of Dyson equations reduces to a set of coupled ordinary differential equations for the atomic state populations, thus making the solution easy to obtain. These simple master equations (SME) could be understood using a golden rule type of argument, so that a very transparent view of the physics emerged. In the limit where the SCA is valid, the calculations of LN based on the SCA showed that intra-atomic correlation between the various pairs of tunneling channels could block the charge transfer.

Unfortunately the SCA is valid only in a limited regime in parameter space. A number of interesting problems, therefore, cannot be treated using the SCA. One such example is He^+ scattering off a Pb surface.[1,4,6,24,25] The kinetic energy of the helium ion in these experiments ranges from 0.4 keV to 2.5 keV, which is outside of the range of validity of the SCA. LN derived more accurate equations, which we call generalized master equations (GME),[26] in order to extend the range of validity of the simple master equations. However, the range of validity of the GME was not fully understood.

It is very important to be able to solve the Dyson equations in a more controlled fashion. In this paper we present a general numerical scheme for the exact solution of the set of Dyson equations. In addition to the instantaneous populations of the atomic states we also calculate the instantaneous nonadiabatic spectral weight

functions of the atomic states. The latter are important for the understanding and prediction of charge transfer dynamics when nonadiabaticity due to the Coulomb correlations will be important.

In Sec. II we formulate the Anderson and slave-boson Hamiltonians for the problem to be solved and write down the self-energies which are now generalized to allow off-diagonality in the atomic state index. We proceed to discuss the instantaneous spectral decomposition for the atomic states. In Sec. III we present an exact numerical scheme to solve the set of coupled Dyson equations. In Sec. IV we present various model calculations for the comparison with results of other theories, and approximations show that our solution describes a wide range of phenomena, and gives sensible results in various limiting cases. We give quantitative predictions for how close to the limits one must be for the limiting forms to be obtained. In particular, we show that thermal equilibrium is approached more slowly than might have been expected, because features near the Fermi level arising from the strong intra-atomic correlations such as the Kondo or mixed valence state[27,28] take a longer time to form than the larger scale features of the spectral density.

II. BASIC THEORY

When atoms scatter against metal surfaces, electrons can tunnel back and forth between the atomic states and the metal's conduction band. Here we treat the motion of the atomic nuclei classically. In reality, the dynamics of the charge transfer is influenced by several factors including (i) the instantaneous energy levels of atomic states relative to the Fermi level of the surface; (ii) the instantaneous tunneling rate between an atomic state and the conduction band of the metal; (iii) nonadiabatic effects due to the finite response time of conduction electrons; (iv) modifications of the classical trajectory when a charge transfer event changes the forces on the atom outside the surface; and (v) quantum effects on atomic motion. Points (i) and (ii) are the properties of the adiabatic or local thermal equilibrium state, and have been recently investigated by Nordlander and Tully.[29] This paper is devoted entirely to point (iii). Some discussions of points (iv) and (v) have been given in the literature. The influence of the electronic processes on the trajectory has been recently discussed by Head-Gordon and Tully.[30] The region of validity of the classical trajectory approximations has been discussed by a number of authors including Brenig,[31] Nourtier,[32] and more recently Burke, Gumhalter, and Langreth.[33]

A. Hamiltonian

We describe the interaction between the atomic states and the metal's conduction electrons by a time-dependent Anderson Hamiltonian,[9,10]

$$H(t)=\sum_{l,\sigma}\varepsilon_{l,\sigma}(t)n_{l,\sigma}+\tfrac{1}{2}{\sum_{}}'U_{l\sigma,l'\sigma'}n_{l\sigma}n_{l'\sigma'}+\sum_{k\sigma}\varepsilon_k n_{k\sigma}+\sum_{l\sigma k}\left[V_{l\sigma k}(t)c^{\dagger}_{k\sigma}c_{l\sigma}+\text{H.c.}\right]. \quad (1)$$

In this equation $\varepsilon_{l\sigma}(t)$ denotes the instantaneous energies of the different atomic levels while ε_k represents the energies (see Appendix A for a more complete discussion of the meaning of $\epsilon_{l\sigma}$) in the continuum of levels in the substrate metal's conduction band.[34] The subscripts σ denote spin for both the atomic states and the conduction electrons, and l and k refer to the spatial quantum numbers of the atom and the metal's conduction electrons, respectively. The components in l and k referring to a common symmetry for both the atom and metal are conserved. The first summation describes the bare atomic states, and the second describes intra-atomic correlation (the primed summation here excludes the term in which both $l=l'$ and $\sigma=\sigma'$). The third summation represents the surface conduction electrons, and the fourth summation describes the tunneling between the atomic states and the surface conduction band of the metal. The abbreviation H.c. denotes the Hermitian conjugate. Equation (1) represents an extension of the conventional Anderson model to the case where multiple atomic orbitals are included. Unless disallowed by symmetry considerations, different atomic orbitals can interact via tunneling to the substrate and back. This results in off-diagonal components of the impurity self-energies and Green's functions, which will be discussed in some detail later in this paper, thus generalizing the equations of Ref. 20.

The importance of the intra-atomic Coulomb interaction U has been discussed previously,[20] and as was done there, we assume that U is sufficiently large that it can be taken to be infinite, so that we can apply the slave-boson method.[20,21] Introducing a creation operator $b^{\dagger}$ satisfying boson commutation relations, we can write the bosonized version of (1) as

$$H(t)=\sum_{l\sigma}\varepsilon_{l\sigma}(t)n_{l\sigma}+\sum_{k}\varepsilon_k n_{k\sigma}+\sum_{l\sigma k}\left[V_{l\sigma k}(t)c^{\dagger}_{k\sigma}b^{\dagger}c_{l\sigma}+\text{H.c.}\right]. \quad (2)$$

In addition to the total electron number, a conserved "charge" Q_B of the above Hamiltonian is given by

$$Q_B\equiv\sum_{l\sigma}n_{l\sigma}+n_B, \quad (3)$$

where $n_B=b^{\dagger}b$. Since only the $Q_B=1$ subspace of (2) is physically relevant, we use the Langreth-Nordlander method[20] for accomplishing the projection onto this subspace.

To treat the nonequilibrium aspects we use the approach introduced by Kadanoff and Baym,[22] in a form summarized by Langreth[35] and used by Langreth and Nordlander (LN).[20] The procedure is to (i) develop an approximation for the self energies, (ii) solve the time-dependent Dyson equation [Eq. (2.9) in LN] for the advanced and retarded Green's functions G^A and G^R, and (iii) solve the Kadanoff-Baym equations for $G^<$ [Eqs. (2.6) and (2.7) in LN] with the appropriate boundary conditions, using the values of G^A and G^R obtained in step (ii). The instantaneous probability $n_i(t)$ for finding an electron in the atomic state $|i\rangle$ is given by the diagonal matrix element

$$n_i(t) = \langle i|G^<(t,t)|i\rangle. \tag{4}$$

In this paper the $|i\rangle$ is either the state $|l\sigma\rangle$ or the slave boson state. Although we typically speak about the n_i's as if they were "populations," we should remember that $G^<$ is thermally averaged over all initial configurations of the substrate electrons, so that more properly n_i is an ensemble average, which, because it is necessarily between 0 and 1 inclusive, can be interpreted as the probability that there is an electron in state $|i\rangle$.

B. Self-energies

We make the same type of approximation for the self-energies as LN. This is diagrammatically represented in Fig. 1, and allows for the generalization to the possibility for nondiagonality in l. As discussed in Appendix B, this approximation is based on an expansion in $1/N$, where N is the effective degeneracy of the atomic level involved. It also contains the leading terms in a perturbation series in the size of the tunneling matrix element V.

We generally follow the notation of LN and use the notation B for the slave boson functions ($>$, $<$, A, or R, that is "greater," "less," advanced, or retarded, as the case may be) and reserve $G_{ll'\sigma}$ for the corresponding atomic state functions and $G_{kk'\sigma}$ for the substrate electron functions. The self-energy term for the atomic states shown in Fig. 1(a) takes the form

$$\Sigma^{\gtrless}_{ll'\sigma}(t,t') = K^{\gtrless}_{ll'\sigma}(t,t')B^{\gtrless}(t,t'), \tag{5}$$

and the self-energy for the slave boson shown in Fig. 1(b) takes the form

$$\Pi^{\gtrless}(t,t') = \sum_{ll'\sigma} K^{\lessgtr}_{l'l\sigma}(t',t)G^{\gtrless}_{ll'\sigma}(t,t'), \tag{6}$$

where $K^{\gtrless}_{ll'\sigma}(t,t')$ is defined in terms of the Green's function for the conduction electrons and the tunneling matrix elements as

$$K^{\gtrless}_{ll'\sigma}(t,t') = \sum_k \bar{V}^*_{l\sigma k}(t)f^{\gtrless}(\varepsilon_k)\bar{V}_{l'\sigma k}(t'), \tag{7}$$

with $\bar{V}_{l\sigma k}(t) = V_{l\sigma k}(t)\exp(i\varepsilon_k t)$. Similarly the advanced and retarded self-energies are given by

$$\Sigma^{R,A}_{ll'\sigma}(t,t') = K^{>}_{ll'\sigma}(t,t')B^{R,A}(t,t'), \tag{8}$$

$$\Pi^{R,A}(t,t') = \sum_{ll'\sigma} K^{<}_{l'l\sigma}(t',t)G^{R,A}_{ll'\sigma}(t,t'). \tag{9}$$

The above quantities have been projected onto the $Q_B = 1$ subspace using the method of LN, according to which one removes all terms of order $(Q_B)^2$ or higher in the "less than" correlation functions.[36] One

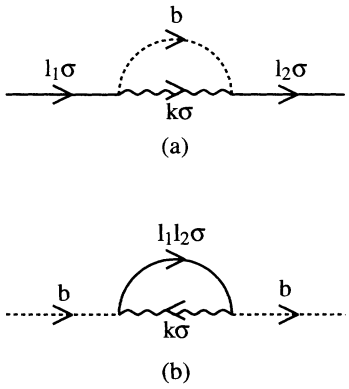

FIG. 1. (a) Self-energy for the atomic state $|l\sigma\rangle$ and (b) self-energy for the slave-boson state. The dashed line denotes the Green's function for the slave-boson state, the wavy line denotes the Green's function for the conduction electrons, and the solid line denotes the Green's functions for an atomic state which can be off-diagonal in the indices l and l'.

aspect of this projection is that we replaced the substrate functions $G^{\gtrless}_{kk'\sigma}(t,t')$ by their unperturbed forms $\delta_{kk'}f^{\gtrless}(\varepsilon_k)\exp(-i\varepsilon_k(t-t'))$ in the expression (7) for $K^{\gtrless}$, where $f^<(\varepsilon)$ is the Fermi function[34] $f^<(\varepsilon) = (e^{\beta\varepsilon}-1)^{-1}$, and $f^>(\varepsilon) = 1 - f^<(\varepsilon)$. Corrections to this are proportional either to $B^<$ or $G^<_{ll'\sigma}$ and hence to $(Q_B)^1$. $K^{\gtrless}$ appears in the Dyson equations of the next section in such a way that any correction to it of order $(Q_B)^1$ causes a correction of order $(Q_B)^2$ to the physical quantities $B^<$ or $G^<_{ll'\sigma}$. Therefore these corrections must be neglected. We emphasize that this neglect, which turns out to be an enormous simplification, is *required*, and is not an additional approximation. This should not be construed to imply that there is no correction to the substrate electron functions themselves, and these do indeed have a correction of order $(Q_B)^1$ which could be used, for example, to calculate the energy transfer to the substrate, an important subject which should be a matter for a future investigation.

Finally it is useful to define

$$\Gamma_{l\sigma}(\varepsilon,t) = 2\pi\sum_k |V_{l\sigma k}(t)|^2\delta(\varepsilon-\varepsilon_k). \tag{10}$$

The quantity

$$\Gamma_{l\sigma}(t) \equiv \Gamma_{l\sigma}(\varepsilon_{l\sigma}(t),t) \tag{11}$$

is a function familiar in the $U = 0$ problem, where to lowest order (see Appendix A) it is the adiabatic tunneling rate from an occupied state $|l\sigma\rangle$ to an empty substrate band. It is useful for setting an overall energy scale, as well as for making contact with *ab initio* single-particle calculations to determine the input parameters of our model.

C. Dyson equations

With the above expressions for the self-energies, the Dyson equations for the atomic states and the slave-boson state can be constructed. Dyson's equation for the advanced or retarded Green's functions [Eq. (2.9) of LN] related

to atomic states $|l\sigma\rangle$ and $|l'\sigma\rangle$ now takes the form

$$\left[i\frac{\partial}{\partial t}-\varepsilon_{l\sigma}(t)\right]G^R_{ll'\sigma}(t,t')=\delta_{l,l'}\delta(t-t')+\sum_{l''}\int_{-\infty}^{\infty}d\bar{t}\,K^{>}_{ll''\sigma}(t,\bar{t})B^R(t,\bar{t})G^R_{l''l'\sigma}(\bar{t},t'), \tag{12}$$

while the Dyson equation for the slave-boson propagator takes the form

$$i\frac{\partial}{\partial t}B^R(t,t')=\delta(t-t')+\sum_{ll'\sigma}\int_{-\infty}^{\infty}d\bar{t}\,K^{<}_{l'l\sigma}(\bar{t},t)G^R_{ll'\sigma}(t,\bar{t})B^R(\bar{t},t'), \tag{13}$$

where $K^{\gtrless}_{ll'\sigma}$ are defined in Eq. (7). The advanced Green's function can be obtained directly from the retarded Green's function using $G^A_{ll'\sigma}(t,t')=(G^R_{l'l\sigma}(t',t))^*$, where the asterisk denotes the complex conjugate.

The Dyson equations for the "less than" Green's functions [Eqs. (2.6) and (2.7) of LN] may be written explicitly using (5) and (8) for the atomic states and (6) and (9) for the slave boson. The "less than" Green's function for the states $|l\sigma\rangle$ and $|l'\sigma\rangle$ satisfies

$$\left[i\frac{\partial}{\partial t}-\varepsilon_{l\sigma}(t)\right]G^<_{ll'\sigma}(t,t')=\sum_{l''}\int_{-\infty}^{\infty}d\bar{t}\,K^{>}_{ll''\sigma}(t,\bar{t})B^R(t,\bar{t})G^<_{l''l'\sigma}(\bar{t},t')+\sum_{l''}\int_{-\infty}^{\infty}d\bar{t}\,K^{<}_{ll''\sigma}(t,\bar{t})B^<(t,\bar{t})G^A_{l''l'\sigma}(\bar{t},t'), \tag{14}$$

while the "less than" Green's function for the slave-boson state satisfies

$$i\frac{\partial}{\partial t}B^<(t,t')=\sum_{ll'\sigma}\int_{-\infty}^{\infty}d\bar{t}\,\left[K^<_{l'l\sigma}(\bar{t},t)G^R_{ll'\sigma}(t,\bar{t})B^<(\bar{t},t')+K^>_{l'l\sigma}(\bar{t},t)G^<_{ll'\sigma}(t,\bar{t})B^A(\bar{t},t')\right]. \tag{15}$$

The Dyson equations can be simplified by introducing $\tilde{G}$ defined by the relation

$$G_{ll'\sigma}(t,t')\equiv\tilde{G}_{ll'\sigma}(t,t')\exp\left[-i\int_{t_0}^{t}d\tau\varepsilon_{l\sigma}(\tau)+i\int_{t_0}^{t'}d\tau\varepsilon_{l'\sigma}(\tau)\right], \tag{16}$$

where t_0 can be any fixed time and G can be a Green's function or $K^{\gtrless}_{ll'\sigma}$ defined in Eq. (7). The retarded Green's functions can be further simplified by introducing $g_{ll'\sigma}(t,t')$ through

$$\begin{aligned}\tilde{G}^R_{ll'\sigma}(t,t')&\equiv -i\theta(t-t')\,g_{ll'\sigma}(t,t'),\\ \tilde{G}^A_{ll'\sigma}(t,t')&\equiv i\theta(t'-t)\,g_{ll'\sigma}(t,t'),\end{aligned} \tag{17}$$

and $b(t,t')$ through

$$\begin{aligned}B^R(t,t')&\equiv -i\theta(t-t')\,b(t,t'),\\ B^A(t,t')&\equiv i\theta(t'-t)\,b(t,t'),\end{aligned} \tag{18}$$

with the supplemental conditions that $g_{ll'\sigma}(t,t)=\delta_{l,l'}$ and $b(t,t)=1$, which arise from the equal-time commutation relations. Notice the following relation:

$$\begin{aligned}g_{ll'\sigma}(t',t)&=g^*_{l'l\sigma}(t,t'),\\ b(t',t)&=b^*(t,t').\end{aligned} \tag{19}$$

In this paper, we calculate the retarded functions and then obtain the advanced ones through complex conjugation, using (17), (18), and (19). The Dyson equations for $g_{ll'\sigma}(t,t')$ and $b(t,t')$ for $t\geq t'$ become

$$\frac{\partial}{\partial t}g_{ll'\sigma}(t,t')=-\sum_{l''}\int_{t'}^{t}d\bar{t}\,\tilde{K}^{>}_{ll''\sigma}(t,\bar{t})b(t,\bar{t})g_{l''l'\sigma}(\bar{t},t'), \tag{20}$$

$$\frac{\partial}{\partial t}b(t,t')=-\sum_{ll'\sigma}\int_{t'}^{t}d\bar{t}\,\tilde{K}^{<}_{l'l\sigma}(\bar{t},t)g_{ll'\sigma}(t,\bar{t})b(\bar{t},t'), \tag{21}$$

which fully determine the functions $g_{ll'\sigma}(t,t')$ and $b(t,t')$ for $t\geq t'$. For $t<t'$ they can then be determined using (19). In this notation the Dyson equations for the "less than" Green's functions take the following form:

$$\frac{\partial}{\partial t}\tilde{G}^<_{ll'\sigma}(t,t')=\sum_{l''}\left[\int_{-\infty}^{t'}d\bar{t}\tilde{K}^<_{ll''\sigma}(t,\bar{t})B^<(t,\bar{t})g^*_{l'l''\sigma}(t',\bar{t})-\int_{-\infty}^{t}d\bar{t}\tilde{K}^>_{ll''\sigma}(t,\bar{t})b(t,\bar{t})\tilde{G}^<_{l''l'\sigma}(\bar{t},t')\right], \tag{22}$$

and

$$\frac{\partial}{\partial t}B^<(t,t') = \sum_{ll'\sigma}\left[\int_{-\infty}^{t'} d\bar{t}\tilde{K}^>_{l'l\sigma}(\bar{t},t)\tilde{G}^<_{ll'\sigma}(t,\bar{t})b^*(t',\bar{t}) - \int_{-\infty}^{t} d\bar{t}\tilde{K}^<_{l'l\sigma}(\bar{t},t)g_{ll'\sigma}(t,\bar{t})B^<(\bar{t},t')\right], \tag{23}$$

where $g^*_{l''l'\sigma}(t',\bar{t})$ and $b^*(t',\bar{t})$, the complex conjugates of $g_{l''l'\sigma}(\bar{t},t')$ and $b(\bar{t},t')$, respectively, are from the advanced Green's functions. The instantaneous population of the atomic state $|l\sigma\rangle$ is then given according to (4) by

$$n_{l\sigma}(t) = \tilde{G}^<_{ll\sigma}(t,t) = G^<_{ll\sigma}(t,t), \tag{24}$$

while the instantaneous population of the slave-boson state is given by

$$n_B(t) = B^<(t,t). \tag{25}$$

It is straightforward to show that $\frac{d}{dt}Q_B(t) = 0$, by using Eqs. (22), (23), (24), (25), and (3), plus the following identity:

$$\frac{dn(t)}{dt} \equiv \frac{\partial}{\partial t}G^<(t,t')\Big|_{t'=t} + \frac{\partial}{\partial t'}G^<(t,t')\Big|_{t'=t}, \tag{26}$$

where n and $G^<$ could either refer to atomic states [Eq. (24)] or the slave boson [Eq. (25)]. Therefore the Dyson equations explicitly conserve Q_B.

D. Spectral decomposition

Here we discuss the spectral density of energies required for the removal of an electron from the state $|l\sigma\rangle$. This is defined as the Fourier transform with respect to $\tau \equiv t - t'$ of $\langle a^\dagger_{l\sigma}(t')a_{l\sigma}(t)\rangle$, where a is the operator that removes a particle from the state $|l\sigma\rangle$ within the $Q_B = 1$ subspace. The operator that does this[21] is $a_{l\sigma} \equiv c_{l\sigma}b^\dagger$, so that

$$A^<_{l\sigma}(t,t') = \langle c^\dagger_{l\sigma}(t')b(t')b^\dagger(t)c_{l\sigma}(t)\rangle. \tag{27}$$

An expression for the spectral density for adding an electron to the state $|l\sigma\rangle$ could be written down in a similar fashion.

The evaluation of the two-particle correlation function (27) in terms of single-particle functions would in general require a further diagrammatic expansion. However, as Coleman[21] has shown, to the order consistent with the self-energy expansions used here (terms of order $1/N$ kept), only the first term in such an expression is required (i.e., vertex corrections are of order $1/N^2$). Its unprojected form is

$$\begin{aligned} A^<_{l\sigma}(t,t') &= G^<_{l\sigma}(t,t')\langle b^\dagger(t')b(t)\rangle \\ &= G^<_{l\sigma}(t,t')b(t',t) + G^<_{l\sigma}(t,t')B^<(t',t), \end{aligned} \tag{28}$$

where $G^<_{l\sigma}(t,t') \equiv G^<_{ll\sigma}(t,t') \equiv \langle c^\dagger_{l\sigma}(t')c_{l\sigma}(t)\rangle$. The last term $G^<_{l\sigma}(t,t')B^<(t',t)$ has a $(Q_B)^2$ dependence and must be projected out. The correctly projected form is then

$$A^<_{l\sigma}(t,t') = G^<_{l\sigma}(t,t')b(t',t). \tag{29}$$

Note that $b(t,t) = 1$, so that

$$A^<_{l\sigma}(t,t) = G^<_{l\sigma}(t,t)b(t,t) = G^<_{l\sigma}(t,t) = n_{l\sigma}(t). \tag{30}$$

Following Kadanoff and Baym[22] we introduce sum and difference variables $T = \frac{1}{2}(t+t')$ and $\tau = t-t'$. The spectral density for occupied states, that is, the probability that an electron removed from state $|l\sigma\rangle$ at time T will have an energy ω, is

$$\rho^{l\sigma}_{\rm occ}(\omega,T) = \frac{1}{2\pi}\int_{-\infty}^{\infty} d\tau\ A^<_{l\sigma}(T+\tau/2, T-\tau/2)\exp[i\omega\tau]. \tag{31}$$

According to (30) the normalization of ρ is given by

$$\int_{-\infty}^{\infty} d\omega\rho^{l\sigma}_{\rm occ}(\omega,T) = n_{l\sigma}(T). \tag{32}$$

In the examples given later, we typically will plot the total occupied spectral weight function for the atomic states, which we define as

$$f_{\rm occ}(\omega,T) = \sum_{l\sigma}\rho^{l\sigma}_{\rm occ}(\omega,T). \tag{33}$$

III. EXACT NUMERICAL SOLUTION

In this section we discuss a numerical scheme which converts the coupled Dyson equations into a set of linear equations for discrete elements. The set of linear equations then will be solved exactly on a time grid using proper boundary and initial conditions. The calculational details are given in Appendix C. Since the advanced and retarded Green's functions are needed in the Dyson equations for the "less than" Green's function, the solution for the advanced and retarded quantities will be presented first.

A. Retarded Green's functions

For a solution to the coupled Dyson equations for the retarded Green's functions, Eqs. (20) and (21) with proper boundary conditions are sufficient. Notice that the integral in Eq. (20) depends on $b(t,\bar{t})$ and $g_{ll'\sigma}(\bar{t},t')$ and the integral in Eq. (21) contains $g_{ll'\sigma}(t,\bar{t})$ and $b(\bar{t},t')$ with $t' < \bar{t} < t$. The Green's functions in the integrals are all located closer to the equal-time direction than (t,t'). Since $g_{ll'\sigma}$ and b at equal time satisfy the boundary condition, it is possible to solve Eqs. (20) and (21) using a discretized representation of the time coordinates.

In the discretized representation the integrals in Eqs. (20) and (21) become sums. The derivatives are

replaced by finite differences. To solve for $g_{ll'\sigma}$ and b at times (m,n) in the discretized representation, one has to rearrange the sums and differences so that $g_{ll'\sigma}$ and b with arguments (m,n) appear on one side of each equation and the Green's functions of other time arguments appear on the other side. As a result, one obtains a set of linear equations for $g_{ll'\sigma}(m,n)$ and $b(m,n)$ depending only on the values of $g_{ll'\sigma}(i,j)$ and $b(i,j)$ with $i-j<m-n$, i.e., closer to the equal time diagonal. Since the values of the Green's functions along the equal-time axis are known, $g_{ll'\sigma}$ and b can be systematically calculated along diagonals parallel to the equal-time direction.

If the discretization is based on a second order implicit scheme, the numerical error going from one grid point to the next is $O([\delta\sqrt{\Gamma_{l\sigma}}]^3)$, where $\Gamma_{l\sigma}$ is the width of the atomic state $|l\sigma\rangle$ defined in Eq. (11). The memory requirements will scale as $O(M^2)$ and the required number of floating point operations will scale as $O(M^3)$, where M is the number of the grid points between $t=\pm\infty$.

In the large Γ and small velocity limit, where M would have to be very large, considerable reduction of the computational effort can result from the observation that the self-energies are strongly localized around equal times. The self-energies contribute significantly only within a region $t-t'<T_c$, thus defining T_c, which we call the *memory time*. The values of the Green's functions at (t,t') with $t>t'$ therefore only depend on the Green's functions in the region (t_1,t_1') with $t-T_c<t_1'<t_1<t$. Thus, the calculation can be performed within a square submatrix of side T_c, provided that the square defining this submatrix moves along the $t=t'$ direction as the calculation proceeds. The computational effort in this limit therefore scales as $N^2\times M$ and the memory requirements will scale as N^2, where N is the number of grid points within T_c.

The above method is also useful for obtaining the thermal equilibrium solution. Here the retarded functions plus thermal occupation probabilities are all that are necessary. The double-time functions depend only on the time difference. Using this fact enables one to set $t\to t-t'$ in the row index and $t'=0$ in the column index of the discretized functions in the numerical Dyson equations. One then obtains closed equations for the elements of the first column and the calculation goes very rapidly, requiring only $O(M)$ in memory size and $O(M^2)$ operations to perform.

B. "Less than" Green's functions

The set of Dyson equations for the "less than" Green's functions can be solved using a technique similar to that used for the retarded Green's functions. Equations (22) and (23) with proper initial conditions are sufficient for obtaining the solution. From Eqs. (22) and (23) it can be seen that the integrals contain the "less than" Green's functions with arguments $t,\bar{t}$ and $\bar{t},t'$ with $-\infty<\bar{t}<t'<t$.[37] This means that the "less than" Green's functions at (t,t') only depend on "less than" Green's functions for times closer to the origin, $t=t'=-\infty$, than (t,t'). Since the initial values of the "less than" Green's functions are known, the Dyson equations of the "less than" Green's functions can be calculated systematically along rows perpendicular to the equal time direction.

If the discretization is based on a second order implicit scheme, the error caused in evaluation of the values at one grid point is $O([\delta\sqrt{\Gamma_{l\sigma}}]^3)$. The required memory and number of operations are the same as those for the calculation of the retarded Green's functions. In the low velocity limit, the localization of the self-energy can be exploited in the same fashion as in the solution of the retarded Green's functions. The calculation can be carried out within a dynamic matrix with side T_c, the memory time, defined as before such that the self-energies become negligible for time arguments differing by more than T_c. This matrix will move along the equal-time direction until $t=\infty$ is reached. The procedure requires $O(N^2)$ in memory and $O(N^2\times M)$ operations.

The combined solutions for the retarded and the "less than" Green's functions define a complete and exact numerical solution to the problem. To minimize memory requirements, one can make use of the fact that $G_{ll'\sigma}(t,t')=[G_{l'l\sigma}(t',t)]^*$,[37] and store both the retarded and the "less than" Green's functions in a single complex square matrix.

In the case of large level width, a variable substitution is performed:

$$x(t)=\int_{-\infty}^{t} d\tau\,\sqrt{\Gamma_{\max}(\tau)}, \tag{34}$$

where $\Gamma_{\max}(\tau)$ denotes the largest $\Gamma_{l\sigma}$ [defined in Eq. (11)] among the $l\sigma$ at the given value of τ. When x is used as the variable, the numerical scheme remains the same, but the error is $O([h_{l\sigma}\delta_x]^3)$ where δ_x is the spacing between adjacent grid points on the x mesh and

$$h_{l\sigma}(x)=\frac{\sqrt{\Gamma_{l\sigma}(x)}}{\sqrt{\Gamma_{\max}(x)}}\le 1, \tag{35}$$

rather than the error $O([\sqrt{\Gamma_{l\sigma}}\delta]^3)$ obtained using t as the independent variable. This variable substitution results in considerable numerical advantages when $\Gamma_{l\sigma}$ is large. To obtain a numerically sound solution with t as the variable, a nonuniform mesh with fine steps in the regions where $\Gamma_{l\sigma}$ is large, and a coarse grid in regions where $\Gamma_{l\sigma}$ is small would be required. A numerical implementation of the present procedure on a nonuniform grid would be realized by variable substitution such as from t to x.

IV. SPECIAL FEATURES AND VARIOUS LIMITING CASES

In the previous sections, the formalism has been described and a numerical algorithm for the solution of the coupled Dyson equations has been presented. In this section, we will investigate some simple limits and the effect of various substrate and atomic parameters on charge transfer.

In the examples given here, we describe everything in

terms of two input functions per atomic level, the time dependent energy position parameter of the atomic level, and time dependent width parameter (see Appendix A and the discussion below). We thus assume that $K_{ll'\sigma}$ [see (7)] is diagonal in l, so that the atomic state functions satisfy $G_{ll'\sigma} = G_{l\sigma}\delta_{ll'}$. We also assume that the k dependence of $V_{l\sigma k}$ is only through $\varepsilon_{l\sigma k}$; finally we assume that the shape of $V_{l\sigma k}$ is invariant. Thus we take $V_{l\sigma k} \equiv v(\varepsilon_k)u_{l\sigma}(t)$. Thus the adiabatic width or tunneling rate function [Eq. (10)] for the $U = 0$ problem can be written

$$\Gamma_{l\sigma}(\varepsilon, t) = 2\pi\rho(\varepsilon)\,|v(\varepsilon)u_{l\sigma}(t)|^2\,. \tag{36}$$

With this definition the sum over k in Eq. (7) becomes an integral and we can write

$$K^{\gtrless}_{ll'\sigma}(t,t') = \delta_{l,l'}\sqrt{\bar{\Gamma}_{l\sigma}(t)\bar{\Gamma}_{l\sigma}(t')}\,f^{\gtrless}(t-t'), \tag{37}$$

where $\delta_{l,l'}$ is the Kronecker δ, and where the bar over the Γ's means that they have been averaged over ϵ. Specifically we let $|v(\varepsilon)|^2\rho(\varepsilon)$ be proportional to a dimensionless shape function $\xi(\varepsilon)$, and define the average $\bar{\Gamma}$ by

$$\bar{\Gamma}_{l\sigma}(t) = \frac{\int \Gamma_{l\sigma}(\varepsilon,t)\,d\varepsilon}{\int \xi(\varepsilon)\,d\varepsilon}. \tag{38}$$

The quantities $f^{\gtrless}(\tau)$ in (37) are then given by

$$f^{\gtrless}(\tau) = \int_{-\infty}^{\infty}\frac{d\varepsilon}{2\pi}\xi(\varepsilon)f^{\gtrless}(\varepsilon)e^{-i\varepsilon\tau}. \tag{39}$$

In the model calculations here we use two different forms of $\xi(\varepsilon)$: (i) a parabolic form $\xi(\varepsilon) = \frac{3}{2}(1 - \varepsilon^2/D^2)$ for $|\varepsilon| \le D$ and $\xi(\varepsilon) = 0$ otherwise, and (ii) a rectangular form $\xi(\varepsilon) = 1$ for $|\varepsilon| \le D$ and $\xi(\varepsilon) = 0$ otherwise. Here ε is being measured with respect to the Fermi level. In either case we will follow convention and use the term "bandwidth" for the quantity $2D$, although it more accurately represents the effective range of energies over which substrate electrons hybridize with an atomic state at the Fermi level, a range which for a conduction electron is cut off by the band bottom at the lower end and a decreasing matrix element at the upper end. The parabolic form is used for all calculations where spectral densities must be obtained, in order to avoid anomalies induced by the unphysical sharp cutoffs in the rectangular ξ. However, the examples where just the charge transfer is calculated are not sensitive to such a cutoff and so the simpler rectangular ξ is used. One must keep in mind, however, that $\Gamma_{l\sigma}(0,t) = \bar{\Gamma}_{l\sigma}(t)$ for the rectangular case, but that $\Gamma_{l\sigma}(0,t) = \frac{3}{2}\bar{\Gamma}_{l\sigma}(t)$ for the parabolic. When discussing the case of N equivalent degenerate levels, where the various quantities are independent of $l\sigma$, we often use the notation Δ. This is defined to coincide with what is normally used in the literature on highly correlated systems as

$$\Delta = \left.\frac{\bar{\Gamma}}{2}\right|_{\varepsilon=0} \tag{40}$$

This means that $\Delta = \frac{\bar{\Gamma}}{2}$ for the rectangular shape function, but $\Delta = \frac{3}{4}\bar{\Gamma}$ for the parabolic one.

In the following model calculations, we also assume that $\bar{\Gamma}_{l\sigma}(t)$ can be parametrized as

$$\bar{\Gamma}_{l\sigma}(t) = \bar{\Gamma}^0_{l\sigma}\exp\left[-\alpha_{l\sigma}Z(t)\right], \tag{41}$$

where $Z(t)$ is the instantaneous position of the nucleus of the atom from the surface at time t and $\bar{\Gamma}^0_{l\sigma}$ and $\alpha_{l\sigma}$ are independent of $Z(t)$. We note that within the band $\Gamma_{l\sigma}(t) = \bar{\Gamma}_{l\sigma}(t)$ for the rectangular shape function $\xi(\varepsilon)$ used by LN, but not for the parabolic shape function used in a few of the examples here.

In addition to $\bar{\Gamma}_{l\sigma}(t)$ the adiabatic level positions $\varepsilon_{l\sigma}(t)$ are input functions. For the atom-surface scattering problems these are parametrized in the following way:

$$\varepsilon_{l\sigma}(t) = b[Z(t) - Z^c_{l\sigma}]. \tag{42}$$

The quantities b and $Z^c_{l\sigma}$ are input parameters, as shown in Fig. 2. In the figures a single integer i, where $i = 1$ or $i = 2$, is used to label the states instead of the $l\sigma$ notation used elsewhere. In many of the model atom-surface scattering applications discussed below, atoms (ions) are assumed to approach the surface in the normal direction at constant velocity until they reach the turning point and then instantly turn around and move away from the surface at the same speed.

A. Semiclassical approximation

The so-called semiclassical approximation (SCA) was developed as an approximate method for the solution of the coupled Dyson's equations.[20] The approximation makes use of the fact that the self-energies $\Sigma(t,t')$ are localized to equal times. The Dyson's equations which are of integro-differential type can thus be converted to differential equations by replacing the Green's functions

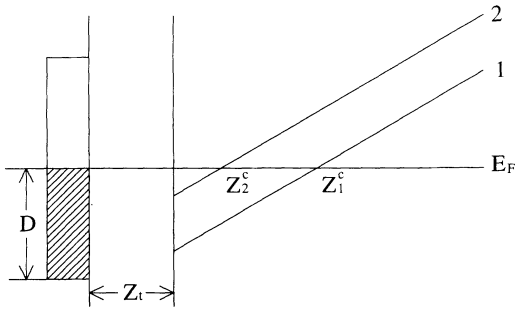

FIG. 2. Schematic illustration of the atomic level shifts along the atomic trajectory outside the surface. E_F is the Fermi energy and D is the distance from the bottom of the band to the Fermi level. We use the rectangular shape function $\xi(\varepsilon)$ for $|v(\varepsilon)|^2\rho(\varepsilon)$. Z^c_1 and Z^c_2 are the points where level 1 and level 2 cross the Fermi level, respectively. The atomic level functions $\varepsilon_1(t)$ and $\varepsilon_2(t)$ are parametrized as in Eq. (42). The $\bar{\Gamma}_1(t)$ and $\bar{\Gamma}_2(t)$ functions are given in Eq. (41). The atom is assumed to move with constant speed towards the surface. At the turning point, Z_t, the atom instantaneously reverses direction and moves outward with the same speed.

in the integrands by their values at the peak of the self-energies. LN showed that this approximation led to two approximate master equations. These are much simpler than the full exact solution, so it is useful to delineate their range of validity precisely, so that they can be used with confidence in this range. That is the aim of this section.

The conditions for the SCA to be valid at low temperature are (LN)

$$\sum_{l\sigma} \frac{\Gamma_{l\sigma}(t)}{|\varepsilon_{l\sigma}(t)|} \ll 1 \tag{43}$$

or

$$\left| \frac{d}{dt} \varepsilon_{l\sigma}(t) \right| \gg \Gamma_{l\sigma}^2(t), \tag{44}$$

where $\Gamma_{l\sigma}(t)$ is the instantaneous adiabatic width of the atomic state defined in Eq. (11), and $\varepsilon_{l\sigma}$ is the energy level of the atomic state with respect to the Fermi energy. The first condition is clearly violated when the atomic energy levels cross the Fermi level. However, if the crossing occurs sufficiently fast so that Eq. (44) is satisfied, the SCA will still be valid. For a given system, the SCA generally works best at high velocities as indicated in Eq. (44). A high temperature will also increase the accuracy of the SCA.[20] However, if one takes a more general perspective and compares different systems that have roughly comparable charge transfers, then one can say that the SCA works better at *low* velocities. This is because according to (43) and (44), the smallness of $\Gamma_{l\sigma}^2$ is the more significant requirement for the validity of the SCA, and the value required for a given charge transfer increases more rapidly than $\left|\frac{d}{dt}\varepsilon_{l\sigma}(t)\right|$ does. In this paper we generally scale $\Gamma_{l\sigma}$ with velocity, which in the simple master equation limit yields a velocity independent charge transfer.

To the lowest order in the SCA limit, the Dyson's equations, Eqs. (22) and (23), can be simplified and the charge transfer dynamics can be described by the following intuitive set of simple master equations (SME):[20]

$$\frac{d}{dt} n_{l\sigma}(t) = -\Gamma_{l\sigma}(t) \Bigg([1 - f(\varepsilon_{l\sigma}(t))] n_{l\sigma}(t) - f(\varepsilon_{l\sigma}(t)) \left[1 - \sum_{l\sigma} n_{l\sigma}(t) \right] \Bigg). \tag{45}$$

The term $[1 - \sum_{l\sigma} n_{l\sigma}(t)]$ describes the available portion of density of states for the atomic state $|l\sigma\rangle$ into which an electron can tunnel. For the zero-U case, this term would be replaced by $[1 - n_{l\sigma}(t)]$. The difference is due to the blocking effect implied by the large intra-atomic correlation term.[20] The SME approach obviously neglects all memory effects in the scattering events. An improved approximation called the "generalized master equation" (GME) [Eq. (3.30) in LN] takes into account some memory effects. A better method for calculating the retarded and advanced functions for use in this equation, and which extends the validity to the finite bandwidth case [or more precisely the case of nonconstant $|v(\varepsilon)|^2 \rho(\varepsilon)$] is derived in Appendix D. It is this version of the GME that is used in the comparisons here.

In Fig. 3 a comparison of the results from the exact solution and the SME solution is plotted. The widths of the atomic levels have been scaled with velocity to keep the total charge-transfer comparable. The results from the SME are therefore independent of velocity. The strong velocity dependence of the charge transfer dynamics from the exact solution suggests that the nonadiabaticity is very important. In Table I, the final populations of the atomic states at various velocities calculated using the exact scheme are listed. It can clearly be seen from Fig. 3 and Table I that the SME works better for lower velocities (in units of the level width).

In Fig. 4 we show a comparison between the results from the exact solution, the GME, and the SME solutions. It can clearly be seen that the GME solution represents a significant improvement on the SME. For both velocities, the GME and the exact solution agrees within 5%. The SME, however, is off by more than 50%.

In Table II, the differences in final populations between the exact solution and the SME described by Eq. (45) and between the exact solution and the GME [Eq. (3.30) in LN's paper[20]] are listed for various parameters. For very low velocities, i.e., $v \leq 10^{-4}$, the results from the exact

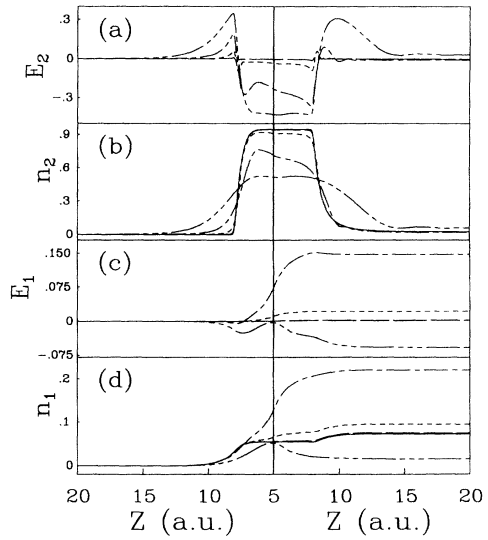

FIG. 3. Comparison of exact solution and the SME at different velocities. Panels (a) and (c) are the absolute differences in the populations for the atomic level 2 and level 1, respectively, calculated using the exact scheme and the SME. Panels (b) and (d) are the populations of the level 2 and level 1, respectively, calculated using the exact scheme and using the SME (solid lines). The long dashed lines are for $v = 10^{-4}$ a.u., the dotted lines for $v = 10^{-3}$ a.u., the dash-dotted lines for $v = 10^{-2}$ a.u., and the dash-triple-dotted lines for $v = 0.1$ a.u. The level shifts are illustrated in Fig. 2. The left half is for the atom approaching the surface and the right half is for the atom leaving the surface. The parameters are taken as $b = 0.02$ a.u., $Z_1^c = 12$ a.u., $Z_2^c = 8$ a.u., $\alpha_1 = 1$ a.u., $\alpha_2 = 0.5$ a.u., $Z_t = 5$ a.u., $\bar{\Gamma}_1^0 = \bar{\Gamma}_2^0 = 100v$, where v is the velocity in atomic units and the half bandwidth $D = 10$ eV. The temperature of the solid is taken as 300 K.

TABLE I. Final populations of atomic states calculated using the exact scheme. Here n_1 and n_2 are the final occupations for atomic state 1 and atomic state 2, respectively.

v (a.u.)	$\to 0$	10^{-4}	10^{-3}	10^{-2}	10^{-1}
n_1	0.0729	0.0725	0.0944	0.2206	0.0232
n_2	0.0259	0.0247	0.0246	0.0180	0.0634

solution, SME, and the GME all agree within 5%.

A detailed analysis of the validity of the GME shows that even for velocities as high as $v = 0.03$, the results from the GME lie within 5% of the results from the exact solution.[26] The original estimate of the validity of the GME (Ref. 20) put an upper bound on the velocity of $v = 10^{-3}$ a.u. The reason the GME produces such good results even at relatively large velocities is that the estimated error is only significant in the region relatively far away from the surface where the atomic level widths are very small. Since there is no charge transfer in this region, the errors are suppressed. For large velocities such as $v = 0.1$ a.u., however, the GME totally breaks down.

We now test the criteria for the SCA, Eqs. (43) and (44) in the above calculation. Let us define $R_t \equiv \sum_{l\sigma} \Gamma_{l\sigma}(t)/|\varepsilon_{l\sigma}(t)|$. At the turning point, $R_t = 63.4 \times v$ for level 1 and $R_t = 148.0 \times v$ for level 2, where v is the velocity. Another quantity of interest is $R_c \equiv \Gamma_{l\sigma}^{-2} \left|\frac{d\varepsilon_{l\sigma}}{dt}\right|$.

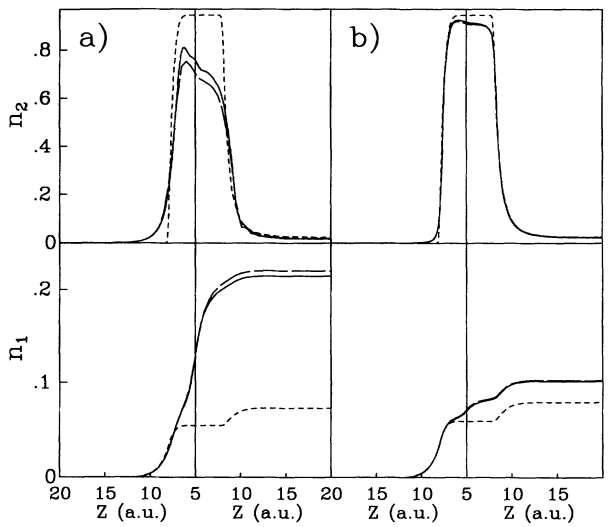

FIG. 4. Comparison of the populations $n_i(Z)$ calculated for large U using the SME, the GME, and the exact solution at different velocities. The parameters of the system are the same as those in Fig. 3. The inputs $\bar{\Gamma}_i^0$ have been scaled for each velocity so that the SME would predict the same charge transfer for each trajectory. The bandwidth of the metal is 0.368 a.u. In (a) we show the results for velocity $v = 0.01$ a.u. and $\Delta_{1,2} = 1$ a.u. In (b) we show the results for velocity $v = 0.001$ a.u. and $\Delta_{1,2} = 0.1$ a.u. The upper part of each figure shows the population $n_1(Z)$ as a function of distance from the surface, while the lower part of the figures shows the population $n_2(Z)$. The dotted lines are the results using the SME, the solid lines are the results using the GME, and the dashed lines are the results obtained using the exact numerical solution.

TABLE II. Percentage deviations of the SME and the GME from the exact scheme. The superscript denotes the SME or the GME while the subscript denotes the atomic state 1 or 2.

v (a.u.)	$\to 0$	10^{-4}	10^{-3}	10^{-2}	10^{-1}
δ_1^{SME}	0.0	2.67	22.8	67.0	214
δ_1^{GME}	0.0	0.56	0.08	2.76	10^4
δ_2^{SME}	0.0	4.98	5.28	43.9	59.1
δ_2^{GME}	0.0	0.53	5.71	4.00	121

At the crossing point, $R_c = 5.3 \times 10^4/v$ for level 1 and $R_c = 6.0 \times 10^{-3}/v$ for level 2. One can see that for $v = 10^{-3}$ and $v = 10^{-4}$, $R_c \gg 1$ and $R_t \ll 1$ are satisfied showing that the SCA should be accurate. For $v = 0.01$, the criteria for the SCA fail for level 2 and are barely satisfied for level 1. The GME at this velocity, however, produces satisfactory results due to the fact that the charge transfer is very small in these regions. For $v = 0.1$, $R_c \gg 1$ only for level 1. The other criteria fail. This is the case where the GME breaks down.

This analysis shows that (i) the GME gives better results than the SCA; (ii) the criteria are much too strict in the sense that the blocking effect and the small atomic population at crossing points are not reflected in the criteria. Our experience with the GME shows that even when the criteria are barely satisfied, the GME produces reasonable results.

B. Finite bandwidth

When the surface bandwidth is finite and the level width is sufficiently narrow that it is spanned entirely by the bandwidth, the spectral weight of the atomic state is largely unaffected by the bandwidth. However, when the atomic level width is large enough to be comparable to or ever larger than the half-bandwidth (the Fermi level to the bottom of the band), the actual spectral weight will be effectively cut off by the finite bandwidth.

In Fig. 5, the instantaneous populations of the upper atomic state and the lower state for some different band cutoffs, i.e., $D = 1.25$ eV, $D = 2.5$ eV, and $D = 5$ eV, are shown, while at the turning point $\bar{\Gamma}_1(Z_t) = 0.18$ eV and $\bar{\Gamma}_2(Z_t) = 2.23$ eV. Since the band cutoffs $D = 2.5$ eV and $D = 5$ eV are larger than the level widths, the dynamics should not be influenced by the bandwidth. From the figure it can clearly be seen that the charge transfer for these bandwidths is very similar. On the other hand, for a band cutoff of $D = 1.25$ eV, which is smaller than $\bar{\Gamma}_2(Z_t) = 2.23$ eV, the dynamics are expected to be different. This can clearly be seen in Fig. 5. For $D = 1.25$ eV, the atomic level width of the upper state is effectively reduced by the small bandwidth. As a result, the upper level becomes more populated in the vicinity of the turning point, $Z_t = 5$ a.u. The population of the lower level is thereby suppressed.

As the bandwidth gets still smaller, one begins to see quantum charge oscillations reminiscent of Stuckelberg oscillations. Since this is the subject of a subsequent

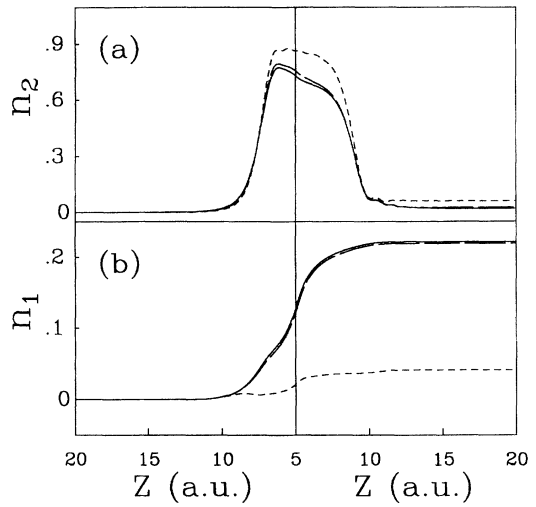

FIG. 5. Instantaneous populations of the atomic states with different bandwidth. The horizontal axis is the distance of the atom from the surface. The left half is for the atom approaching the surface and the right half is for the atom leaving the surface. Panel (a) is for the population of the upper level and panel (b) for the population of the lower level. The solid lines are for the half bandwidth $D = 5$ eV, the long dashed lines for $D = 2.5$ eV, and the dotted lines for $D = 1.25$ eV. The atomic level shift functions vary linearly as in Fig. 2. The parameters are taken as $b = 0.02$ a.u., $Z_1^c = 12$ a.u., $Z_2^c = 8$ a.u., $\alpha_1 = 1$ a.u., $Z_t = 5$ a.u., and $\bar{\Gamma}_1^0 = \bar{\Gamma}_2^0 = 1$ a.u. The $\bar{\Gamma}$ values at the turning point are $\bar{\Gamma}_1(Z_t) = 0.18$ eV, and $\bar{\Gamma}_2(Z_t) = 2.23$ eV, respectively.

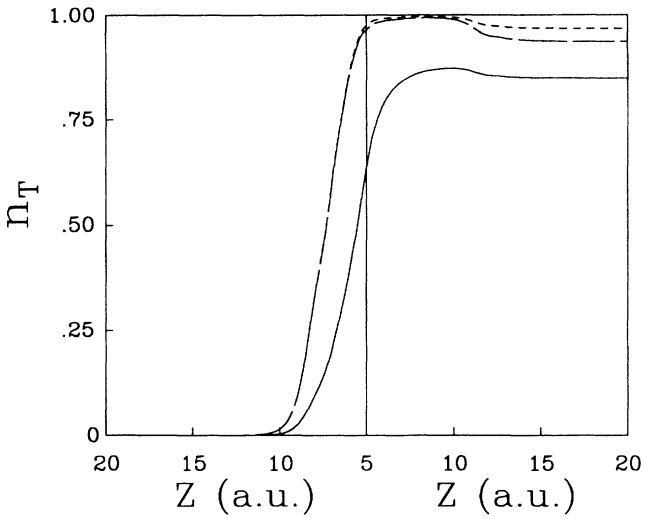

FIG. 6. Total instantaneous population of the atom for large U. The solid line is for $N = 1$, the long dashed line is for $N = 2$, and the dotted line is for $N = 4$. The atomic trajectory is as described in Fig. 2. The levels are assumed degenerate with $Z_c = 10$ a.u. and $\alpha_i = 0.7$ a.u. The velocity is $v = 0.01$ a.u. and the half bandwidth is $D = 10$ eV. At the turning point, $Z_t = 5$ a.u., we take $N\bar{\Gamma}(Z_t) = 0.82$ eV, where N is the degeneracy. The atom is assumed to begin moving towards the surface at a distance of 20 a.u. from the surface and to turn back away from the surface at $Z_t = 5$ a.u.

paper,[25] we will not discuss the narrow bandwidth limit further here, but simply mention that this is another limiting case which is described correctly by the theory.

C. The effect of degeneracy

In this section we investigate the effects of degeneracy of the atomic levels on the charge transfer. In the traditional theories for the charge transfer, where intra-atomic correlation effects have been neglected,[10,11] the charge transfer probability depends only on the total width of the atomic state. We will show that there are cases where the detailed tunneling rate of each individual channel can have a significant effect on the dynamics even though the total tunneling rate is kept constant.

In Fig. 6 the instantaneous population of an atomic level is plotted for the degeneracies $N = 1$, $N = 2$, and $N = 4$, where the $N = 1$ results are taken from the $U = 0$ theory, which is exact in this case. It can clearly be seen that the final charge transfer is larger for higher degeneracy. The final populations of the atomic levels for these three cases are 0.85 for $N = 1$ and 0.94 and 0.97 for $N = 2$ and $N = 4$, respectively. If the incoming beam consisted of singly charged positive ions, then typically one measures the fraction that remain ions on output, i.e., $1 - n$, which varies according to the above prediction by a factor of 5 as N is increased from 1 to 4.

We now turn to a system in equilibrium and calculate the occupied spectral weight as a function of N. The results are shown in Fig. 7. For $N = 1$ the result is of course just the Fermi-function truncated Lorentzian-like curve of the $U = 0$ theory. As N increases the highly correlated Kondo or mixed valence peak rises at the Fermi level. Most of the weight for this peak comes from the lower energy part of the spectrum rather than from a substantial change of the atomic occupation number which has the values $n \approx 0.79$ for $N = 1$, $n \approx 0.79$ for $N = 2$, and $n \approx 0.81$ for $N = 4$.

A relevant parameter in determining whether or not a sharp peak appears near the Fermi level when the atomic level is below the Fermi level is the Kondo temperature T_K. The width of the peak is $\sim T_K$ and it virtually disappears when the ratio βT_K of the Kondo temperature T_K to the temperature β^{-1} becomes much less than unity. Although $|\varepsilon|$ is not strictly in the Kondo regime

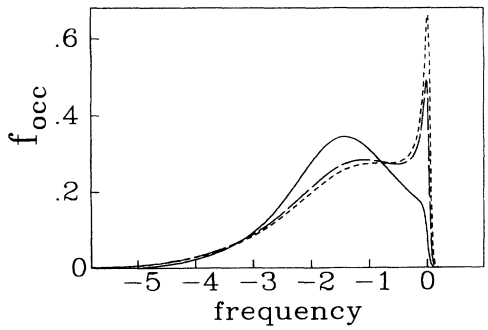

FIG. 7. Total occupied spectral weight function, as defined in Eq. (33). The solid curve is for the single level, the long dashed curve for $N = 2$, and the dotted curve for $N = 4$. The half-bandwidth is taken as $D = 5N\Delta$, $\beta^{-1} = 0.026N\Delta$, and $\epsilon = -N\Delta$. The abscissa is in units of $N\Delta$.

$n \approx 1$, it is still useful to estimate T_K (Appendix E). For the situation depicted in Fig. 7, we find $T_K = 0.067N\Delta$ for $N = 4$ and $T_K = 0.044N\Delta$ for $N = 2$. For comparison $\beta^{-1} = 0.026N\Delta$ in each case. Therefore we are in a regime where the temperature is lower than the other energy scales of the problem, and the widths of the Fermi level resonances should be $\sim T_K$, and that is indeed the case.

D. The approach to equilibrium

A nontrivial question for any nonequilibrium theory is how long it will take a prepared initial configuration to return to thermal equilibrium. Improperly formulated theories may not show a return to equilibrium at all. We illustrate here both in the Kondo and the mixed valent regimes that the instantaneous occupied spectral weight function [Eq. (31)] does in fact return to its thermal equilibrium value, once the Hamiltonian becomes time independent. We calculate the time necessary for this relaxation to equilibrium.

In Fig. 8 the nonequilibrium occupied spectral weight functions of an atomic state for large time T and the equilibrium one calculated by Coleman's projection method[21] are compared for different paths towards final equilibrium in the mixed valence regime as well as in the the Kondo regime. In Fig. 8(a) the final atomic energy is in the mixed valence regime with $N = 2$. T_K is estimated at $0.067N\Delta$ while the temperature is $0.026N\Delta$. The thick dotted curve coincides with the solid line showing that the level has indeed reached thermal equilibrium. Figure 8(b) shows similar results for the case where the equilibrium state is in the Kondo[27] regime with $N = 6$. Here we estimate $T_K = 0.003N\Delta$, while the temperature is $0.0046N\Delta$.

What about the question of how long it takes? Relevant here is what we call the memory time T_c, which we define to be the interval $(t, t + T_c)$ outside of which the retarded self-energies in Eqs. (8) and (9) becomes negligible. It is shown in Fig. 8(a) that the "less than" Green's function takes a longer time than the retarded Green's function to reach final equilibrium. In the particular calculation for Fig. 8(a), it is sufficient to take the memory time $T_c = 100(N\Delta)^{-1}$ with Δ defined in Eq. (40). In order to simplify the picture, the problem is modeled in the following way: the level width starting as zero and increasing exponentially until it reaches its final value. The long dashed curve in Fig. 8(a) is the instantaneous occupied spectral weight function when the nonequilibrium retarded Green's functions first become identical to the equilibrium ones. When the parameters of a system remain constant for a time longer than the memory time, the equilibrium and nonequilibrium retarded Green's functions will be identical because the Dyson equations and boundary conditions at equal time for the nonequilibrium and equilibrium functions are equivalent. The fact that the long dashed curve is different from the equilibrium curve shows that the occupied spectral weight function takes a longer time to reach its equilibrium by a factor of 4, for this particular model calculation.

E. Local thermal equilibrium and deviations

We now investigate the conditions under which local thermal equilibrium can be maintained if the system is driven by a slow time variation of the level position. How slow a variation is necessary to maintain thermal equilibrium? The answer is crucial to all fundamental calculations of dynamics, because it will tell us whether the electronic motion follows the nuclear motion adiabatically or not, or in other words whether the Born-Oppenheimer approximation can be used or not.

All parameters of the system except the position of the atomic level will be kept constant. We define the local thermal equilibrium as the equilibrium state corresponding to the instantaneous position of the atomic level. We take the time (T) variation of the atomic energy level to

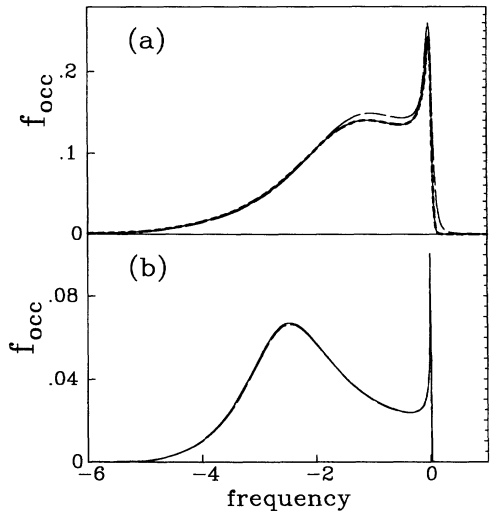

FIG. 8. The approach to equilibrium. The solid curves are the instantaneous "nonequilibrium" spectral weight functions of the atomic states for time $T \gg T_c$. The thick dotted curve in panel (a) and the dashed curve in panel (b) are the corresponding thermal equilibrium spectral functions. The dashed line is the instantaneous nonequilibrium spectral function calculated at an intermediate time $T = T_c$ after the time dependent $\bar{\Gamma}$ becomes constant. The thick dotted curve in panel (a), taken at $T = 4T_c$ after the time dependent $\bar{\Gamma}$ becomes constant, coincides with the solid curve. The vertical axis measures the occupied spectral weight function and the horizontal axis measures the frequency in the units of $N\Delta_c$ with N the degeneracy of the atomic states and Δ_c the final equilibrium value of Δ [Eq. (40)]. Panel (a) is for $N = 2$, the final energy level of an atomic state $\varepsilon = -N\Delta_c$, the half conduction bandwidth $D = 5N\Delta_c$, the temperature of the solid $\beta^{-1} = 0.026N\Delta_c$, a temperature corresponding, for example, to 300 K for $N\Delta_c = 1$ eV. The height of the energy level stays constant, while the position dependent $\Delta(z)$ is parametrized by $\Delta(z) = \Delta_c \exp[-\alpha(z - z_c)]$ for $z > z_c$ and $\Delta(z) = \Delta_c$ for $z < z_c$, where $\alpha(z_0 - z_c) \gg 1$, and where z_0 is the starting point. Panel (b) is for $N = 6$, $\varepsilon = -2N\Delta$, $D = 5N\Delta$, and $\beta^{-1} = 0.0046N\Delta$. The energy levels of the atomic states start their motion very high above the Fermi energy and quickly approach their final equilibrium value while the values of Δ are kept constant. The parabolic shape function $\xi(\varepsilon)$ is used.

be[34]

$$\varepsilon_\sigma(T) = \varepsilon_\sigma - b_\sigma T, \tag{46}$$

where ε_σ is the initial energy of the atomic state. Both ε_σ and b_σ are taken as constants. The quantity Δ is kept constant during the process and the temperature $\beta^{-1} = 0.026N\Delta$. Our calculation shows that when $\left|\frac{d}{dT}\varepsilon_\sigma(T)\right| \leq 0.025\ (N\Delta)^2$, the instantaneous occupied spectral weight functions differ imperceptibly from their equilibrium counterparts. This implies that the local thermal equilibrium is maintained. In the present calculation we will assume a level shift of $\left|\frac{d}{dT}\varepsilon_\sigma(T)\right| = 0.25\ (N\Delta)^2$.

In Fig. 9, we show some snapshots of the system just described. It can clearly be seen that the difference between the instantaneous spectral functions and the corresponding local thermal equilibrium plots are largest when the atomic level lies close to the Fermi energy. It is also in the energy range close to the Fermi energy that the largest deviations from local thermal equilibrium occur. The mixed-valence and the Kondo peaks are much weaker than their local thermal equilibrium counterparts. The widths of these resonance peaks are relatively narrow,

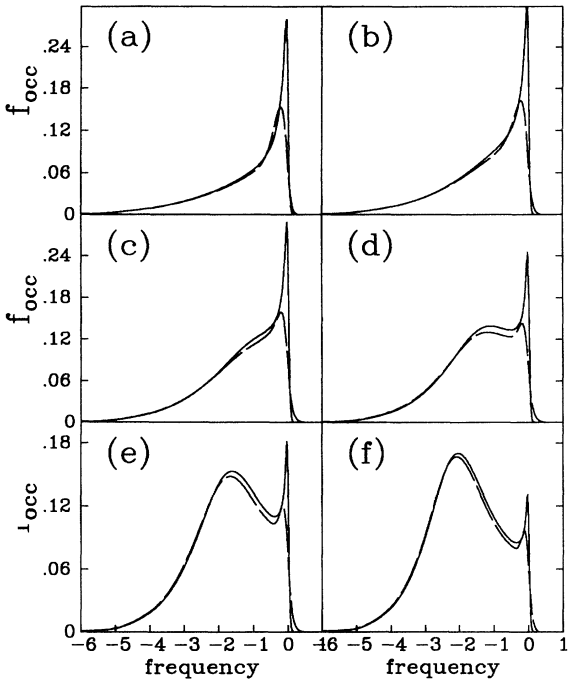

FIG. 9. Local thermal equilibrium. The solid curves are the occupied spectral weight functions of the system in local thermal equilibrium. The long dashed curves are the instantaneous occupied spectral weight functions. The $\bar{\Gamma}$ function (and hence Δ) is kept time independent and the rate of change of the atomic energy level position $\left|\frac{d}{dT}\varepsilon_\sigma(T)\right| = 0.25(N\Delta)^2$. The degeneracy N is given by $N = 2$. Panels (a) to panel (f) show $\rho_{l\sigma}(\omega, T)$ at times T when $\varepsilon_{l\sigma}(T)/N\Delta$ equals -0.1, -0.4, -0.7, -1.0, -1.3, and -1.6, respectively. The energy or frequency on the abscissa is measured from the Fermi level and in units $N\Delta$. The temperature was $0.026N\Delta$ and $D = 5N\Delta$. The abscissa is in units of $N\Delta$.

suggesting that they should take a longer time to form. With the present rate of variation of the atomic level position, there is not enough time for the resonance peak to be fully formed.

In the final snapshot, we are at a point where the T_K is becoming less than the temperature. The Fermi level resonance is disappearing, and local equilibrium is much better maintained in the region of what is left of this resonance. By the time ε reaches $-2N\Delta$ we find that the resonance has all but disappeared.

We conclude from our model calculation that if a system varies with time sufficiently slowly, local thermal equilibrium can be maintained. When local thermal equilibrium does break down, it is going to do so first near the Fermi energy. The fact that there can be anomalously sharp features in this region due to the Kondo or mixed valent states is likely to attach special importance to this region.

We close this subsection by discussing a possible channel for enhanced nonadiabatic energy transfer between atom and surface induced by the formation of the resonance peak near the Fermi energy of the atomic spectral function. There are two channels of energy transfer in atom surface scattering: excitation of surface phonons and excitation of electron-hole pairs in the surface. Because of the unfavorable mass ratio, electron-hole pair excitation via slow atomic motion can be of importance only when sharp energy features move near the Fermi level.[11,31,33] The conventional descriptions of energy loss due to the excitation of electron-hole pairs have been based on a single-level Anderson model. In the $U = 0$ model, an enhancement of the nonadiabaticity can occur only when the atomic level passes the Fermi energy, because only then is there a sharp feature near the Fermi level in atomic spectral function. For large correlation cases, as has been shown in this and the preceding subsections, many-body effects strongly enhance the spectral weight just below the Fermi energy by forming a sharp resonance peak. This occurs even when the atomic level is located well below the Fermi level in the Kondo regime and even when the width Γ is sufficiently large that there would be little electron-hole pair excitation even if the atomic level were near the Fermi level. The strong increase in spectral weight below the Fermi energy induced in the Kondo and mixed valence regime is likely to enhance the probability of nonadiabatic electron-hole pair formation. Further studies are needed to evaluate the importance of this nonadiabatic energy transfer mechanism.

V. CONCLUSIONS

We have presented a general many-body description of charge transfer in atom-surface scattering including the effects of large intra-atomic correlation. This is a generalization of the theory of LN to include off-diagonal atomic self-energies and an arbitrary "bandwidth" and shape as a function of energy for the adiabatic single electron tunneling rate into the substrate. A very important result is that we have developed an exact numerical solution to these equations. This was used to put quantitative nu-

merical limits on the region where the much simpler simple or generalized master equations developed in LN were valid, and it was found that this region was considerably larger than the simple *a priori* criteria would have led one to expect. The exact solution was also used to investigate the "bandwidth" dependence of the charge transfer; significant changes were found as the bandwidth was sufficiently narrowed. It was shown that increasing the degeneracy of a single atomic level did not lead to a significant reduction in the atomic occupation probability, although it did lead to a substantial rearrangement of the weight in the instantaneous spectral functions as the Kondo and mixed valence resonances rose near the Fermi level. We found the time required for a fixed atomic species outside the surface to return to its equilibrium charge state, and determined how fast such an atom could move and still remain in local thermal equilibrium. It was found in regimes where the mixed valence or Kondo state are present that the Fermi level resonances representing these states could not be maintained in local thermal equilibrium except for anomalously slow atom velocities. This is a source of nonadiabatic charge transfer, and hence nonadiabatic energy transfer, which is not present in previous models. The extent to which this nonadiabaticity will have important effects on atomic motions is unknown, but should be investigated.

ACKNOWLEDGMENTS

This work was supported in part by the National Science Foundation under Grants Nos. DMR 91-03466 (D.C.L. and H.S.) and DMR 91-17479 (P.N.). Acknowledgment is made to the donors of the Petroleum Research Fund, administered by the American Chemical Society for the partial support of this research, under Grants No. 21723-AC5 (D.C.L. and H.S.) and 27240-AC5 (P.N.). We thank T. Brunner and P. Coleman for a useful conversation.

APPENDIX A: MEANING OF INPUT PARAMETERS

Normally in a realistic calculation one would like to take the input parameters, $\varepsilon_{l\sigma}$ and $\Gamma_{l\sigma}$, from a static one-body calculation of the *ab initio* type, so it is useful to discuss the relationship between these parameters and the single-particle energies and widths determined in such a calculation. For the case discussed earlier (LN) of a single level and a flat substrate band with large bandwidth, the quantities ε and Γ [see Eq. (11)] are just the single-particle energy and width (FWHM or decay rate) obtained from the one-body calculation. This is no longer exactly true in the case considered here, however. For finite bandwidth, or a nonflat band, or where there are multiple levels which are close enough in energy to affect each other's decay rates, one must determine the parameters by comparing the solution of the static $U = 0$ Anderson model with the *ab initio* calculation.

It suffices to obtain the retarded Green's function, whose poles determine the energies and decay rates of the states in terms of the ε's and Γ's. This is most conveniently done in frequency space, where we can just write down the exact retarded self-energy as

$$\Sigma_{ll'}(\omega) = \sum_k V_{lk}^* \frac{1}{\omega - \varepsilon_k} V_{l'k}, \tag{A1}$$

where the index σ has been dropped since the spin channels are not coupled in the single-particle picture. In addition, we deal only with retarded functions here, so that we drop the "R" superscript. To obtain $G_{ll'}(\omega)$ we must invert the matrix $(\omega - \varepsilon_l)\delta_{ll'} - \Sigma_{ll'}(\omega)$. One obtains

$$G_{ll}(\omega) = \frac{1}{\omega - \varepsilon_l - \Lambda_{ll}(\omega)}, \tag{A2}$$

where $\Lambda_{ll'}(\omega)$ is obtained by solving

$$\Lambda_{ll'}(\omega) = \Sigma_{ll'}(\omega) + \sum_{l''} \Sigma_{ll''}(\omega) \times \frac{1 - \delta_{l''l'}}{\omega - \varepsilon_{l''} - \Sigma_{l''l''}(\omega)} \Lambda_{l''l'}(\omega). \tag{A3}$$

If there is but a single l channel, then $\Sigma_{ll}(\omega) = \Lambda_{ll}(\omega)$ and (omitting the subscripts) one finds in the vicinity of the pole

$$G(\omega) = \frac{Z}{\omega - E + i/2\tau}, \tag{A4}$$

where E is obtained by solving $E = \varepsilon + \mathrm{Re}\,\Sigma(E)$, Z is given by $Z = \left[1 - \frac{\partial}{\partial E}\mathrm{Re}\Sigma(E)\right]^{-1}$, and $1/\tau = Z\,\mathrm{Im}\,\Gamma(E) \equiv -2Z\,\mathrm{Im}\,\Sigma(E)$, where a real argument to a function implies the limit toward that value from above the real axis. The quantities E and τ are the adiabatic energy and lifetime as determined by one-body theory and are the appropriate quantities to fit to such a calculation. For a wide flat band, $\mathrm{Re}\Sigma$ is essentially zero, and one obtains $E = \varepsilon$ and $1/\tau = \Gamma(\varepsilon)$ as in (11). However if the band is finite or energy varying, then the above process must be inverted to find ε and Γ.

For the case of multiple levels, one then needs to solve (A3) or else show that the difference between Σ and Λ is negligible. It will not be negligible for levels whose widths overlap, as is likely to be the case for levels which are degenerate in the absence of the surface, but which become coupled as the atom moves toward the surface. The retarded Green's function will now in the simplest wide band case have a pole in the lower half plane for each state. One solves for the position and residues of these poles and carries out the earlier procedure for each one. This is straightforward for the case of two states where one can do everything analytically, and the procedure can also be easily inverted to find ε_l and Γ_l from a given set of E_l and τ_l, if one makes the factorization assumption with the same shape function for each state. For larger numbers of coupling states, where numerical methods would be necessary, the procedure would become quite tedious.

APPENDIX B: DISCUSSION OF APPROXIMATIONS

As mentioned in the text, the basic truncation of the exact self-energy to what is shown in Fig. 1 is appro-

priate to leading order in $1/N$ and to second order in V, where N is the effective number of degenerate states on the atom, and V is the tunneling matrix element of the Hamiltonian (1). With respect to N variation, one compares different problems with different N which otherwise have roughly the same gross energy scales. In this problem the gross energy scale is set by the initial rate of filling of all the atomic states together, given that they are all empty. This rate is related to the slave boson self-energy and is proportional to NV^2. Since this is to remain constant as we vary N, it is useful[21] to define a rescaled (N-independent) hopping matrix element $\tilde{V}$ through $V = \tilde{V}/\sqrt{N}$. In this way it is easy to see that one order higher in V^2 means one higher order in $1/N$ if the vertex summations are fully restricted by conservation of $l\sigma$ and the same order in $1/N$ if totally unrestricted. This is how the demonstrations of the correctness of the procedure are carried out.[21] The only difference here is that there are never any fully restricted sums, because the l labels do not all refer to conserved quantum numbers, even though the σ labels always do. Therefore the *effective* N for our problem, although larger than the number of elements in the σ space (normally two), will be smaller than the number of elements in the $l\sigma$ space combined. Without an exact specification of the particular problem to be solved, it is not possible to define the effective N more precisely. The imposition of constraint to the $Q_B = 1$ subspace further complicates the issue in a well known way.[27,28]

We mention that the theory as presented is also self-consistent, conserving, and "Φ derivable" in the sense of Baym,[38] which guarantees, for example, that all Ward identities are satisfied. This, and the fact that it is a non-perturbative theory that is appropriate when N is large and T not too small,[27,28] put an important constraint on the theory making it unlikely that unreasonable results will be predicted even if N is not so large. This is important because one certainly wants to apply the theory to cases where N is as small as 2. Here a $1/N^2$ correction would be estimated at 25%. The only place where the validity can be checked with certainty is for the case $N = 1$, where the smallness of $1/N$ cannot reasonably be invoked, but for which the theory compares very favorably in the cases we have checked with the exact $N = 1$ theory (i.e., the $U = 0$ theory), except that the Fermi level resonances, which in this case would be spurious, although becoming very small, do not disappear entirely.

In actual applications it may be desirable to make further approximations or simplifying assumptions, which are not actually necessary in order to enable the application of the exact solution method given in Sec. III, and indeed such a simplification was made in Sec. IV, where we illustrate the application of the exact solution to various cases. This was to neglect the nondiagonality of $K^{\gtrless}_{ll'\sigma}$ in l. The first thing to note is that the off-diagonal atomic Green's functions are smaller by a factor of $1/N$ with respect to the diagonal ones. However, they make a contribution to the slave boson propagator of order $1/N$, and therefore, except for very large N, the neglect of these terms would need to be justified by means other than the $1/N$ expansion, presumably via the sizes of the matrix elements and energy differences in the particular problem under consideration. One might expect that these terms would have to be kept if the states l and l' had nearby energies and were not of different symmetry, because then small energy denominators would appear.

APPENDIX C: DETAILS OF THE EXACT NUMERICAL SOLUTION

In this appendix, the Dyson equations are discretized and the method of solution presented.

1. The retarded Green's functions

Here we will use the discrete integers i, j, m, and n in place of the time arguments of the various functions, with consecutive integers representing a time difference of δ, the grid spacing. The discretized version of Eqs. (20) and (21) can be written as

$$g_{ll'\sigma}(m,n) = g_{ll'\sigma}(m-1,n) - \sum_{l''} \tfrac{1}{2}\delta^2 \sum_{i=m-1}^{m} \sum_{j=n}^{i} c_j \tilde{K}^{>}_{ll''\sigma}(i,j) b(i,j) g_{l''l'\sigma}(j,n), \tag{C1}$$

and

$$b(m,n) = b(m-1,n) - \sum_{ll'\sigma} \tfrac{1}{2}\delta^2 \sum_{i=m-1}^{m} \sum_{j=n}^{i} c_j \tilde{K}^{<}_{l'l\sigma}(j,i) g_{ll'\sigma}(i,j) b(j,n), \tag{C2}$$

where c_j equals unity except when $j = n$ or i, where $c_j = \frac{1}{2}$.

The quantities $g_{ll'\sigma}(m,n)$ and $b(m,n)$ inside the summation on the right hand sides of Eqs. (C1) and (C2) can be moved over to the left side. Using the fact that $g_{ll'\sigma}(m,m)$ and $b(m,m)$ are unity, one can rewrite Eqs. (C1) and (C2) in the following way:

$$g_{ll'\sigma}(m,n) + \sum_{l''} \tfrac{1}{4}\delta^2 \tilde{K}^{>}_{ll''\sigma}(m,m) g_{l''l'\sigma}(m,n) + \tfrac{1}{4}\delta^2 \tilde{K}^{>}_{ll'\sigma}(m,n) b(m,n)$$

$$= g_{ll'\sigma}(m-1,n) - \tfrac{1}{4}\delta^2 \tilde{K}^{>}_{ll'\sigma}(m-1,n) b(m-1,n) - \sum_{l''} G_{ll'l''\sigma}(m,n), \tag{C3}$$

and

$$\sum_{ll'\sigma} \tfrac{1}{4}\delta^2 \tilde{K}^{<}_{l'l\sigma}(n,m) g_{ll'\sigma}(m,n) + \left[1 + \tfrac{1}{4}\delta^2 \sum_{l\sigma} \tilde{K}^{<}_{ll\sigma}(m,m)\right] b(m,n)$$
$$= b(m-1,n) - \sum_{l\sigma} \tfrac{1}{4}\delta^2 \tilde{K}^{<}_{ll\sigma}(m-1,m-1) b(m-1,n) - \sum_{ll'\sigma} B_{ll'\sigma}(m,n). \quad \text{(C4)}$$

In this expression $G_{ll'l''\sigma}(m,n)$ is defined as

$$G_{ll'l''\sigma}(m,n) = \tfrac{1}{4}\delta^2 \tilde{K}^{>}_{ll''\sigma}(m-1,m-1) g_{l''l'\sigma}(m-1,n) + \tfrac{1}{2}\delta^2 \sum_{i=m-1}^{m} \sum_{j=n+1}^{i-1} \tilde{K}^{>}_{ll''\sigma}(i,j) b(i,j) g_{l''l'\sigma}(j,n) \quad \text{(C5)}$$

and $B_{ll'\sigma}(m,n)$ as

$$B_{ll'\sigma}(m,n) = \tfrac{1}{4}\delta^2 \tilde{K}^{<}_{l'l\sigma}(n,m-1) g_{ll'\sigma}(m-1,n) + \tfrac{1}{2}\delta^2 \sum_{i=m-1}^{m} \sum_{j=n+1}^{i-1} \tilde{K}^{<}_{l'l\sigma}(j,i) g_{ll'\sigma}(i,j) b(j,n). \quad \text{(C6)}$$

The set of Dyson equations for continuous Green's functions have now been converted into a set of linear equations of discrete Green's functions. Since the equal time values of the Green's functions are known, the discrete Green's functions can be obtained in the following manner. (i) Set the values of $g_{ll'\sigma}$ to be $\delta_{l,l'}$ and b to be unity along the diagonal. (ii) Solve $g_{ll'\sigma}(m,m+n)$ and $b(m,m+n)$ for all possible m with fixed n. (iii) Increase n by 1 and repeat step (ii) until all elements in the matrix are solved.

The order in which steps (ii) and (iii) are taken is not unique. As long as the calculations are arranged in such a way that all the values of Green's functions in Eqs. (C5) and (C6) have been previously obtained, the linear equations for the discrete Green's function can be solved. The particular order given here is the one that can be most easily vectorized.

2. The "less than" Green's functions

The "less than" Green's functions can be calculated from the discretized version of Eqs. (22) and (23) and their conjugate equations. For $t \neq t'$, the discretized and simplified version of Eq. (22) can be written as

$$\tilde{G}^{<}_{ll'\sigma}(m,n) + \sum_{l''} \tfrac{1}{4}\delta^2 \tilde{K}^{>}_{ll''\sigma}(m,m) \tilde{G}^{<}_{l''l'\sigma}(m,n) - \tfrac{1}{4}\delta^2 \tilde{K}^{<}_{ll'\sigma}(m,n) B^{<}(m,n)$$
$$= \tilde{G}^{<}_{ll'\sigma}(m-1,n) + \tfrac{1}{4}\delta^2 \tilde{K}^{<}_{ll'\sigma}(m-1,n) B^{<}(m-1,n) + \sum_{l''} G_{ll'l''\sigma}(m,n). \quad \text{(C7)}$$

The discretized and simplified version of Eq. (23) can be expressed as

$$-\sum_{ll'\sigma} \tfrac{1}{4}\delta^2 \tilde{K}^{>}_{l'l\sigma}(n,m) \tilde{G}^{<}_{ll'\sigma}(m,n) + \left[1 + \sum_{l\sigma} \tfrac{1}{4}\delta^2 \tilde{K}^{<}_{ll\sigma}(m,m)\right] B^{<}(m,n)$$
$$= B^{<}(m-1,n) - \sum_{l\sigma} \tfrac{1}{4}\delta^2 \tilde{K}^{<}_{ll\sigma}(m-1,m-1) B^{<}(m-1,n) + \sum_{ll'\sigma} B_{ll'\sigma}(m,n). \quad \text{(C8)}$$

In these expressions,

$$G_{ll'l''\sigma}(m,n) = \tfrac{1}{2}\delta^2 \sum_{i=m-1}^{m} \left[\sum_{j=1}^{n-1} \tilde{K}^{<}_{ll''\sigma}(i,j) B^{<}(i,j) g^{*}_{l'l''\sigma}(n,j) - \sum_{j=1}^{i-1} \tilde{K}^{>}_{ll''\sigma}(i,j) b(i,j) \tilde{G}^{<}_{l''l'\sigma}(j,n)\right]$$
$$-\tfrac{1}{4}\delta^2 \tilde{K}^{>}_{ll''\sigma}(m-1,m-1) \tilde{G}^{<}_{l''l'\sigma}(m-1,n), \quad \text{(C9)}$$

and

$$B_{ll'\sigma}(m,n) = \tfrac{1}{2}\delta^2 \sum_{i=m-1}^{m} \left[\sum_{j=1}^{n-1} \tilde{K}^{>}_{l'l\sigma}(j,i) \tilde{G}^{<}_{ll'\sigma}(i,j) b^{*}(n,j) - \sum_{j=1}^{i-1} \tilde{K}^{<}_{l'l\sigma}(j,i) g_{ll'\sigma}(i,j) B^{<}(j,n)\right]$$
$$+\tfrac{1}{4}\delta^2 \tilde{K}^{>}_{l'l\sigma}(n,m-1) \tilde{G}^{<}_{ll'\sigma}(m-1,n). \quad \text{(C10)}$$

These expressions were simplified by moving the "less than" Green's functions at m, n to the left side of the equations, and keeping the "less than" Green's functions at i, j with $i + j < m + n$ on the right side.

Equations (C7) and (C8) are used to calculate the off-diagonal "less than" Green's functions. For $t = t'$, to ensure the conservation of Q_B, Eqs. (C7) and (C8) as well as their conjugate equations are needed. Using the relation (26), we find that the equal-time components of the Green's functions satisfy

$$\frac{d}{dt}\tilde{G}^{<}_{ll'\sigma}(t,t) = 2\,\mathrm{Re}\sum_{l''}\int_{-\infty}^{t} d\bar{t}\left[\tilde{K}^{<}_{l''l\sigma}(\bar{t},t)B^{<}(\bar{t},t)g_{l'l''\sigma}(t,\bar{t}) - \tilde{K}^{>}_{ll''\sigma}(t,\bar{t})b(t,\bar{t})\tilde{G}^{<}_{l''l'\sigma}(\bar{t},t)\right], \tag{C11}$$

and

$$\frac{d}{dt}B^{<}(t,t) = 2\,\mathrm{Re}\sum_{ll'\sigma}\int_{-\infty}^{t} d\bar{t}\left[\tilde{K}^{>}_{l'l\sigma}(t,\bar{t})\tilde{G}^{<}_{ll'\sigma}(\bar{t},t)b(t,\bar{t}) - \tilde{K}^{<}_{l'l\sigma}(\bar{t},t)g_{ll'\sigma}(t,\bar{t})B^{<}(\bar{t},t)\right]. \tag{C12}$$

In these expressions, $g_{ll'\sigma}$ and b are the simplified retarded Green's functions calculated using the algorithm described in the preceding subsection. Here $g^{*}_{ll'\sigma}$ and b^{*} are the complex conjugates of $g_{ll'\sigma}$ and b, respectively.

For the diagonal (equal time) "less than" Green's functions, Eqs. (C11) and (C12) can be discretized and simplified to the following forms:

$$\tilde{G}^{<}_{ll'\sigma}(m,m) + \mathrm{Re}\sum_{l''}\tfrac{1}{2}\delta^2\tilde{K}^{>}_{ll''\sigma}(m,m)\tilde{G}^{<}_{l''l'\sigma}(m,m) - \mathrm{Re}\tfrac{1}{2}\delta^2\tilde{K}^{<}_{l'l\sigma}(m,m)B^{<}(m,m)$$

$$= \tilde{G}^{<}_{ll'\sigma}(m-1,m-1) + \mathrm{Re}\left[\tfrac{1}{2}\delta^2\tilde{K}^{<}_{l'l\sigma}(m-1,m-1)B^{<}(m-1,m-1) + \sum_{l''}G_{ll'l''\sigma}(m)\right], \tag{C13}$$

and

$$-\mathrm{Re}\sum_{ll'\sigma}\tfrac{1}{2}\delta^2\tilde{K}^{>}_{l'l\sigma}(m,m)\tilde{G}^{<}_{ll'\sigma}(m,m) + \left[1 + \mathrm{Re}\sum_{l\sigma}\tfrac{1}{2}\delta^2\tilde{K}^{<}_{ll\sigma}(m,m)\right]B^{<}(m,m)$$

$$= B^{<}(m-1,m-1) - \mathrm{Re}\left[\sum_{l\sigma}\tfrac{1}{2}\delta^2\tilde{K}^{<}_{ll\sigma}(m-1,m-1)B^{<}(m-1,m-1) + \sum_{ll'\sigma}G_{ll'l'\sigma}(m)\right]. \tag{C14}$$

In these expressions $G_{ll'l''\sigma}(m)$ is given by

$$G_{ll'l''\sigma}(m) = \delta^2\sum_{i=m-1}^{m}\left[\sum_{j=1}^{i-1}\tilde{K}^{<}_{l''l\sigma}(j,i)B^{<}(j,i)g_{l'l''\sigma}(i,j) - \sum_{j=1}^{i-1}\tilde{K}^{>}_{ll''\sigma}(i,j)b(i,j)\tilde{G}^{<}_{l''l'\sigma}(j,i)\right]$$
$$-\tfrac{1}{2}\delta^2\tilde{K}^{>}_{ll''\sigma}(m-1,m-1)\tilde{G}^{<}_{l''l'\sigma}(m-1,m-1). \tag{C15}$$

Notice that Eqs. (C13) and (C14) lead to the relation $\sum_{l\sigma}\tilde{G}^{<}_{ll\sigma}(m,m) + B^{<}(m,m) = \sum_{l\sigma}\tilde{G}^{<}_{ll\sigma}(m-1,m-1) + B^{<}(m-1,m-1)$. The conservation of Q_B is thus preserved exactly in the discrete representation.

The solution to the set of linear equations for the "less than" Green's functions can be obtained using the following prescription. (i) Initialize $G^{<}_{ll'\sigma}(1,1)$ with the original population of the atomic state for $l = l'$ and with zero for $l \neq l'$ and $B^{<}(1,1)$ with 1 minus the sum of the original populations of all the atomic states. (ii) Solve $G^{<}_{ll'\sigma}(m-n,n)$ and $B^{<}(m-n,n)$ for all possible n with fixed m. (iii) Repeat step (ii) with m starting at 3 and increasing by 1 at a time until (M,M) is reached. M is the number of points along one direction of the matrix and corresponds to the total time between effective $t = \pm\infty$. Again steps (ii) and (iii) can be rearranged. The algorithm given above is suitable for vectorization.

APPENDIX D: SIMPLE AND GENERALIZED MASTER EQUATIONS

The self-energies $\Sigma(t,t')$ are strongly localized to equal times. The SCA amounts to replacing the Green's functions in the integrands of the right-hand side of the Dyson equations by their values at the peak of the self-energies.

Applying the SCA to the Dyson equations (22) and (23) results in the following equations:

$$\frac{\partial}{\partial t}\tilde{G}^{<}_{ll'\sigma}(t,t') = \sum_{l''}\left[B^{<}(t,t)\int_{-\infty}^{t'} d\bar{t}\tilde{K}^{<}_{ll''\sigma}(t,\bar{t})g^{*}_{l'l''\sigma}(t',\bar{t}) - \tilde{G}^{<}_{l''l'\sigma}(t,t')\int_{-\infty}^{t} d\bar{t}\tilde{K}^{>}_{ll''\sigma}(t,\bar{t})b(t,\bar{t})\right] \tag{D1}$$

and

$$\frac{\partial}{\partial t}B^{<}(t,t') = \sum_{ll'\sigma}\left[\tilde{G}^{<}_{ll'\sigma}(t,t)\int_{-\infty}^{t'} d\bar{t}\tilde{K}^{>}_{l'l\sigma}(\bar{t},t)b^{*}(t',\bar{t}) - B^{<}(t,t')\int_{-\infty}^{t} d\bar{t}\tilde{K}^{<}_{l'l\sigma}(\bar{t},t)g_{ll'\sigma}(t,\bar{t})\right]. \tag{D2}$$

These equations are standard partial differential equations and can be solved relatively straightforwardly once the retarded Green's functions have been calculated. To make the approximations more transparent, the retarded and advanced Green's functions are now introduced. Using Eqs. (37), (17), and (18) and omitting the off-diagonal Green's function in l, the Dyson equations (D1) and (D2) take the form

$$i\frac{\partial}{\partial t}\tilde{G}^{<}_{\sigma}(t,t') = \tilde{G}^{<}_{\sigma}(t,t')\int_{-\infty}^{t} d\bar{t}\sqrt{\bar{\Gamma}_{\sigma}(t)\bar{\Gamma}_{\sigma}(\bar{t})}\,\tilde{f}^{>}_{\sigma}(t,\bar{t})B^{R}(t,\bar{t}) + B^{<}(t,t)\int_{-\infty}^{t'} d\bar{t}\sqrt{\bar{\Gamma}_{\sigma}(t)\bar{\Gamma}_{\sigma}(\bar{t})}\,\tilde{f}^{<}_{\sigma}(t,\bar{t})\tilde{G}^{A}_{\sigma}(\bar{t},t') \tag{D3}$$

and

$$i\frac{\partial}{\partial t}B^{<}(t,t') = B^{<}(t,t')\sum_{\sigma}\int_{-\infty}^{t} d\bar{t}\sqrt{\bar{\Gamma}_{\sigma}(t)\bar{\Gamma}_{\sigma}(\bar{t})}\,\tilde{f}^{<}_{\sigma}(\bar{t},t)\tilde{G}^{R}_{\sigma}(t,\bar{t}) + \sum_{\sigma}\tilde{G}^{<}_{\sigma}(t,t)\int_{-\infty}^{t'} d\bar{t}\sqrt{\bar{\Gamma}_{\sigma}(t)\bar{\Gamma}_{\sigma}(\bar{t})}\,\tilde{f}^{>}_{\sigma}(\bar{t},t)B^{A}(\bar{t},t'). \tag{D4}$$

In order to evaluate these expressions, approximate expressions for the advanced and retarded Green's functions must be derived. Applying the SCA to the Dyson equations for the advanced and retarded Green's functions Eqs. (20) and (21) and making use of Eqs. (37), (17), and (18), the following Dyson equations are obtained:

$$i\frac{\partial}{\partial t}\tilde{G}^{R}_{\sigma}(t,t') = \delta(t-t') + \tilde{G}^{R}_{\sigma}(t,t')\int_{-\infty}^{\infty} d\bar{t}\sqrt{\bar{\Gamma}_{\sigma}(t)\bar{\Gamma}_{\sigma}(\bar{t})}\,\tilde{f}^{>}_{\sigma}(t,\bar{t})B^{R}(t,\bar{t}) \tag{D5}$$

and

$$i\frac{\partial}{\partial t}B^{R}(t,t') = \delta(t-t') + B^{R}(t,t')\sum_{\sigma}\int_{-\infty}^{\infty} d\bar{t}\sqrt{\bar{\Gamma}_{\sigma}(t)\bar{\Gamma}_{\sigma}(\bar{t})}\,\tilde{f}^{<}_{\sigma}(\bar{t},t)\tilde{G}^{R}_{\sigma}(t,\bar{t}). \tag{D6}$$

These equations can be integrated to obtain the following expressions for the retarded Green's functions:

$$\begin{aligned}\tilde{G}^{R}_{\sigma}(t,t') &= \frac{\theta(t-t')}{i}\exp\left[-i\int_{t'}^{t} d\tau\int_{t'}^{\tau} d\bar{t}\sqrt{\bar{\Gamma}_{\sigma}(\tau)\bar{\Gamma}_{\sigma}(\bar{t})}\,\tilde{f}^{>}_{\sigma}(\tau,\bar{t})B^{R}(\tau,\bar{t})\right],\\ B^{R}(t,t') &= \frac{\theta(t-t')}{i}\exp\left[-i\sum_{\sigma}\int_{t'}^{t} d\tau\int_{t'}^{\tau} d\bar{t}\sqrt{\bar{\Gamma}_{\sigma}(\tau)\bar{\Gamma}_{\sigma}(\bar{t})}\,\tilde{f}^{<}_{\sigma}(\bar{t},\tau)\tilde{G}^{R}_{\sigma}(\tau,\bar{t})\right].\end{aligned} \tag{D7}$$

Due to the localization of $\tilde{f}^{\gtrless}$ the $d\bar{t}$ integral can be extended to $-\infty$. To lowest order, one can then replace the retarded Green's functions in the exponents by

$$\begin{aligned}\tilde{g^{0}}^{R}_{\sigma}(t,t') &= \frac{\theta(t-t')}{i}\exp\left[-\int_{t'}^{t} d\tau\int_{t'}^{\tau} d\bar{t}\sqrt{\bar{\Gamma}_{\sigma}(\tau)\bar{\Gamma}_{\sigma}(\bar{t})}\,\tilde{f}^{>}_{\sigma}(\tau,\bar{t})\right],\\ {b^{0}}^{R}(t,t') &= \frac{\theta(t-t')}{i}\exp\left[-\sum_{\sigma}\int_{t'}^{t} d\tau\int_{t'}^{\tau} d\bar{t}\sqrt{\bar{\Gamma}_{\sigma}(\tau)\bar{\Gamma}_{\sigma}(\bar{t})}\,\tilde{f}^{<}_{\sigma}(\bar{t},\tau)\right].\end{aligned} \tag{D8}$$

We thus obtain the expressions

$$\begin{aligned}\tilde{G}^{R}_{\sigma}(t,t') &= \frac{\theta(t-t')}{i}\exp\left[-i\int_{t'}^{t} d\tau\int_{t'}^{\tau} d\bar{t}\sqrt{\bar{\Gamma}_{\sigma}(\tau)\bar{\Gamma}_{\sigma}(\bar{t})}\,\tilde{f}^{>}_{\sigma}(\tau,\bar{t}){b^{0}}^{R}(\tau,\bar{t})\right],\\ B^{R}(t,t') &= \frac{\theta(t-t')}{i}\exp\left[-i\sum_{\sigma}\int_{t'}^{t} d\tau\int_{t'}^{\tau} d\bar{t}\sqrt{\bar{\Gamma}_{\sigma}(\tau)\bar{\Gamma}_{\sigma}(\bar{t})}\,\tilde{f}^{<}_{\sigma}(\bar{t},\tau)\tilde{g^{0}}^{R}_{\sigma}(\tau,\bar{t})\right]\end{aligned} \tag{D9}$$

for the retarded Green's functions. These expressions represent an improvement on the expressions in Eq. (3.28) of LN, which were derived for infinite bandwidth.

Equations (D9) can be inserted directly into Eq. (D3) and the Dyson equations can be solved by direct integration. Notice that since $Q_B = 1$, the slave boson population can be calculated directly from

$$n_B(t) = 1 - \sum_{\sigma} n_{\sigma}(t). \tag{D10}$$

The populations of the impurity levels can be directly calculated from Eqs. (D3).

Using the identity (26), rate equations for the populations of the impurity states can be derived directly from Eq. (D3) and take the form

$$\frac{d}{dt}n_\sigma(t) = n_\sigma(t)2\,\mathrm{Im}\left[\int_{-\infty}^{t} d\bar{t}\sqrt{\bar{\Gamma}_\sigma(t)\bar{\Gamma}_\sigma(\bar{t})}\tilde{f}_\sigma^{>}(t,\bar{t})B^R(t,\bar{t})\right] + n_B(t)2\,\mathrm{Im}\left[\int_{-\infty}^{t} d\bar{t}\sqrt{\bar{\Gamma}_\sigma(t)\bar{\Gamma}_\sigma(\bar{t})}\tilde{f}_\sigma^{<}(t,\bar{t})\tilde{G}_\sigma^A(\bar{t},t)\right], \tag{D11}$$

where Eq. (D9) is used for the advanced and retarded Green's functions. These equations will be referred to as the generalized master equations (GME) and can be solved straightforwardly. Detailed comparisons between the exact calculation and the results from the GME for different velocities and bandwidths have been described elsewhere.[26] The GME well describe the charge transfer for ion-surface scattering in the hyperthermal regime.

Further simplifications in the spirit of the SCA are possible.[26] Assuming that the rapid oscillation with respect to $\bar{t}$ is contained in the functions $\tilde{f}^{\gtrless}$, we obtain

$$\frac{d}{dt}n_\sigma(t) = -\Gamma_\sigma(t)\left[f^{>}(\epsilon_\sigma(t))n_\sigma(t) - f^{<}(\epsilon_\sigma(t))n_B(t)\right]. \tag{D12}$$

This equation is referred to as the simple master equation (SME).

APPENDIX E: ESTIMATION OF THE KONDO TEMPERATURE

For the multichannel Anderson model (no off-diagonal terms in the atomic level index) and a rectangular $\xi(\epsilon)$ one can make use of the Bethe ansatz to solve for T_K analytically; for ϵ in the band the result[39] may be written as

$$T_K = D\exp\left(-\frac{\pi|\epsilon|}{N\Delta} - \alpha\right), \tag{E1}$$

where $\alpha = \alpha_\infty + \delta\alpha$, with

$$\alpha_\infty = \ln 2\pi - 1 - C \approx 0.260\,66 \tag{E2}$$

and

$$\delta\alpha = \frac{1}{N}\left(\frac{1}{2} + \ln\frac{\pi|\epsilon|}{N\Delta}\right), \tag{E3}$$

where C is Euler's constant. To obtain an approximate generalization to a parabolic band, we note first that as long as Δ is the value at the Fermi level the leading exponent $\pi\epsilon/N\Delta_F$ will be unchanged and we assume that the formula (E1) is still valid at least approximately, if we replace the bandwidth D by an effective bandwidth D'. Using the logarithmic scaling appropriate to the Kondo problem gives

$$\ln\frac{D'}{D} = \int_{-D}^{0}\frac{d\varepsilon}{\varepsilon}\left[\frac{\xi_r(\varepsilon)}{\xi_r(0)} - \frac{\xi_p(\varepsilon)}{\xi_p(0)}\right] = -\frac{1}{2}, \tag{E4}$$

where ξ_r refers to the rectangular shape function and ξ_p refers to the parabolic one. This suggests that we can still use (E1) for the parabolic band as long as we make the replacement $D \to De^{-\frac{1}{2}}$, which is the same as using $\alpha_\infty = 0.760\,66$ instead of (E2). All the Kondo temperatures estimated in this paper will use this procedure.

Equations (E1), (E2), and (E3) can also be used to estimate the validity of the $1/N$ expansion in the Kondo region by expanding the exponent in (E1) to order $1/N$ and comparing how the result differs from the exact one. In this manner one estimates, for example, for the parameter choices in Fig. 7, that the results are in error by about 10% for $N = 4$ and 60% for $N = 2$. As $|\varepsilon/N\Delta|$ gets larger, so does the error, so that we estimate a 10% error for a case with the parameters of Fig. 8(b) even for $N = 6$.

[1] R. L. Erickson and D. P. Smith, Phys. Rev. Lett. **34**, 297 (1975).
[2] H. H. Brongersma and T. M. Buck, Surf. Sci. **53**, 649 (1975).
[3] T. W. Rusch and R. L. Erickson, J. Vac. Sci. Technol. **13**, 374 (1976).
[4] W. Heiland and E. Taglauer, Nucl. Instrum. Methods **132**, 535 (1976).
[5] N. H. Tolk *et al.*, Phys. Rev. Lett. **36**, 747 (1976).
[6] J. C. Tully, Phys. Rev. B **16**, 4324 (1977).
[7] G. A. Kimmel, D. M. Goodstein, and B. H. Cooper, J. Vac. Sci. Technol. A **7**, 2186 (1989).
[8] K. D. Tsuei, P. D. Johnson, P. Nordlander, and D. C. Langreth, Phys. Rev. B **47**, 4142 (1993).
[9] P. W. Anderson, Phys. Rev. **124**, 41 (1961).
[10] A. Blandin, A. Nourtier, and D. Hone, J. Phys. (Paris) **37**, 369 (1976).
[11] R. Brako and D. M. Newns, Rep. Prog. Phys. **52**, 655 (1989).
[12] R. Brako and D. M. Newns, Solid State Commun. **55**, 633 (1985).
[13] W. Bloss and D. Hone, Surf. Sci. **72**, 277 (1978).
[14] T. B. Grimley, V. C. J. Bhasu, and K. L. Sebastian, Surf. Sci. **124**, 305 (1983).
[15] A. Yoshimori, H. Kawai, and K. Makoshi, Prog. Theor. Phys. Suppl. **80**, 203 (1984).
[16] K. L. Sebastian, Phys. Rev. B **31**, 6976 (1985).
[17] K. W. Sulston, A. T. Amos, and S. G. Davison, Phys. Rev. B **37**, 9121 (1988).
[18] P. Nordlander and N. Lang, Phys. Rev. B **44**, 13 681 (1991).
[19] P. Nordlander, Phys. Rev. B **46**, 2584 (1992).
[20] D. C. Langreth and P. Nordlander, Phys. Rev. B **43**, 2541

(1991).
[21] P. Coleman, Phys. Rev. B **29**, 3035 (1984).
[22] L. P. Kadanoff and G. Baym, *Quantum Statistical Mechanics* (Benjamin, New York, 1962).
[23] L. V. Keldysh, Zh. Eksp. Teor. Fiz. **47**, 1515 (1964) [Sov. Phys. JETP **20**, 1018 (1965)].
[24] S. Schippers *et al.*, Surf. Sci. **257**, 289 (1991).
[25] H. Shao, D. C. Langreth, and P. Nordlander, following paper, Phys. Rev. B **49**, 13 948 (1994).
[26] H. Shao, D. C. Langreth, and P. Nordlander, in *Low Energy Ion-Surface Interactions*, edited by J. W. Rabalais (John Wiley & Sons, Ltd., Sussex, 1994), p. 117.
[27] H. R. Krishnamurthy, J. W. Wilkins, and K. G. Wilson, Phys. Rev. B **21**, 1044 (1980); N. E. Bickers, Rev. Mod. Phys. **59**, 845 (1987).
[28] A. C. Hewson, *The Kondo Problem to Heavy Fermions* (Cambridge University Press, Cambridge, 1993).
[29] P. Nordlander and J. C. Tully, Phys. Rev. Lett. **61**, 990 (1988).
[30] M. Head-Gordon and J. C. Tully, Surf. Sci. **268**, 113 (1992).
[31] W. Brenig, Z. Phys. B **38**, 81 (1979).
[32] A. Nourtier, J. Phys. (Paris) **46**, 55 (1985).
[33] K. Burke, B. Gumhalter, and D. C. Langreth, Phys. Rev. B **47**, 12 852 (1993).
[34] We measure single particle energies from the Fermi energy E_F. We measure frequencies, energies, and temperatures in the same units, so that $\hbar$ and k_B never appear.
[35] D. C. Langreth, in *Linear and Nonlinear Electron Transport in Solids*, edited by J. T. Devreese and V. E. van Doren (Plenum, New York, 1976).
[36] For the atomic and slave boson functions the projection is most easily implemented by keeping only the terms in the respective Dyson equations that have the same power law dependence on Q_B on both sides: $(Q_B)^0$ for the retarded and advanced equations and $(Q_B)^1$ for the "less than" equations.
[37] The relation $t > t'$ is always assumed because the Green's function at (t', t) equals the complex conjugate of the Green's function at (t, t').
[38] G. Baym, Phys. Rev. **127**, 1391 (1962).
[39] J. W. Rasul and A. C. Hewson, J. Phys. C **17**, 3337 (1984).